Fluid Phase Equilibria 560 (2022) 113519

Contents lists available at ScienceDirect

Fluid Phase Equilibria

journal homepage: www.journals.elsevier.com/fluid-phase-equilibria

Viscosity measurements of CO_2-rich; $CO_2 + N_2$ and $CO_2 + H_2$ mixtures in gas or supercritical phase at temperatures between 273 and 473 K and pressures up to 8.7 MPa

Bahareh Khosravi [a,*], Benjamin Betken [b], Jana P. Jakobsen [a], Sigurd W. Løvseth [c], Roland Span [b]

[a] Department of Chemical Engineering, Norwegian University of Science Technology (NTNU), NO-7491, Trondheim, Norway
[b] Lehrstuhl für Thermodynamik, Ruhr-Universität Bochum, D-44780, Bochum, Germany
[c] SINTEF Energy Research, P.O. Box 4761 Sluppen, NO-7465, Trondheim, Norway

ARTICLE INFO

Keywords:
CO_2
Viscosity
Binary mixtures
Rotating body viscometer
CCS

ABSTRACT

New experimental viscosity data of three binary CO_2-rich mixtures with approximate mole fractions of 0.93 CO_2 + 0.07 H_2, 0.80 CO_2 + 0.20 H_2, and 0.90 CO_2 + 0.10 N_2 are reported. The measurements were performed at four different isotherms between 273 K and 473 K. Two independent rotating body viscometers with different pressure range were utilized, suitable for measurement of pressures up to 2 MPa and 20 MPa, respectively. The maximum expanded combined relative uncertainty ($k = 2$) in viscosity was 0.25% for the data obtained from the low-pressure viscometer and 0.6% for the data measured by the high-pressure viscometer. The experimental data were compared to the data estimated by the extended corresponding states (ECS) model implemented in the NIST REFPROP 10.0 database. The maximum deviation between the model and the new data is 1.86%. The data measured with the two apparatuses agree within the estimated uncertainty.

1. Introduction

In CO_2 capture, transport, and storage (CCS), the knowledge of the thermophysical properties is crucial for safe and cost-effective design, optimization, and operation of processes [1–4]. Accurate thermophysical data can be used to build accurate models to predict the behavior of the fluids [5], or to verify a specific process condition. The dynamic viscosity is a key property in flow and heat transfer models. This fluid property is needed, e.g., for the estimation of the pressure drop and pipeline diameter, the pump or compressor power consumption, and the performance of heat exchangers [6].

In reservoir modeling, the viscosity is essential to estimate plume evolution and major parameters such as reservoir injectivity and storage efficiency [5–7]. The viscosity of pure CO_2 is rather well-known. However, the impact of impurities on the viscosity of CO_2 streams cannot be neglected, in particular for CO_2 transport and storage processes [8–10]. Even small uncertainties in viscosity might significantly increase the uncertainty of process simulation models [11]. Such uncertainties can lead to costly overdesign in CO_2 transport and/or risks of inefficient or unreliable CO_2 injection and storage.

As of today, there are knowledge gaps in data for the thermophysical properties of CO_2 with impurities needed to develop accurate property models [5, 6]. Among different potential impurities, H_2 is a relevant component when CCS is implemented in blue hydrogen production [12]. Nitrogen is also an important impurity present in many CO_2 sources and capture processes. The available experimental data on viscosity for CO_2 + H_2 mixtures are summarized in Table 1. As can be seen, most of the data are not covering the temperature and pressure regions of interest for CCS. The data measured by [13–17] are limited to atmospheric pressure, close to the ambient temperature or to a single temperature/pressure condition. The data by Refs. [15,18] were measured at a higher pressure range, but the maximum mole fraction of CO_2 is 0.4, which is not relevant for most CO_2 transport and storage applications. There are very little data for CO_2-rich mixtures. For instance, no data below 500 K was reported in Ref. [18], and Ref. [19] provides data in liquid phase but only at one composition. In addition, the given uncertainty of 1% is questionable since only the uncertainty in pressure measurements has been considered. The data situation for $CO_2 + N_2$ mixtures, provided in Table 2 is similar. The existing data are limited to ambient temperatures except the data by Kestin et al. [20], which extend up to 800 K, but only at a single pressure. The data set recently published by Humberg et al. [21] has improved the data situation for $N_2 + CO_2$

* Corresponding author.
E-mail address: bahareh.khosravi@ntnu.no (B. Khosravi).

https://doi.org/10.1016/j.fluid.2022.113519
Received 21 January 2022; Received in revised form 30 May 2022; Accepted 31 May 2022
Available online 1 June 2022

Table 1
Experimental literature data on the viscosity of $CO_2 + H_2$ mixtures; where T is the temperature, p is the pressure, and x_{CO2} is the mole fraction of CO_2. Different types of uncertainty are reported in each source.

Source	T / K	p/ MPa	x_{CO2}	No. of data points	Method of measurement	Reported uncertainty
Trautz and Kurz (1931) [13]	298 - 550	0.1	0.11 – 0.88	24	Capillary	-
Buddenberg and Wilke (1951) [14]	298	0.1	0.25 – 0.75	5	Capillary	-
Golubev and Petrov (1959) [15]	286 & 323	0.1 – 15	0.05 – 0.25	15	Capillary	-
Saksena and Saxena (1965) [22]	300 - 550	0.1	0.21 -0.80	11	Capillary	
Gururaja et al. (1967) [16]	297 & 300	0.1	0.37 – 0.9	5	Oscillating disk	-
Kestin et al. (1983) [17]	295 & 303	0.1	0.32 – 0.79	6	Oscillating disk	±0.1%
Mal'tsev et al. (2004) [18]	500 - 1100	0.3	0.15 – 0.85	15	Capillary	3%
Al-Siyabi (2013) [19]	280 - 343	8.73 - 48.26	0.95	51	Capillary	1%
Cheng et al. (2020) [23]	286 & 673	2 – 30	0.30 – 0.40	34	Capillary	0.05% ($k = 2$)

Table 2
Experimental literature data on the viscosity of binary $CO_2 + N_2$ mixtures; where T is the temperature, p is the pressure, and x_{CO2} is the mole fraction of CO_2.

Source	T / K	p / MPa	x_{CO2}	No. of data points	Method of measurement	Reported uncertainty u
Kestin et al. (1959) [24]	293	1 - 2.13	0.10 – 0.90	46	Oscillating disk	0.05%
Golubev (1959) [15]	289		2 – 12		Capillary	-
Kestin et al. (1966) [25]	293 & 303	1 - 2.53	0.07 – 0.80	23	Oscillating disk	±0.1%
Gururaja et al. (1967) [16]	295 – 303	0.098	0.22 – 0.80	7	Oscillating disk	-
Munczak, and Hochrainer [26]	288 - 323	0.1	0 - 1	90	Capillary	-
Kestin et al. (1974) [20]	298 – 873	1	0.20 – 0.82	28	Oscillating disk	± 0.1%- 0.3%
Humberg et al. (2020) [21]	253 – 473	up to 20	0.25 – 0.75	287	Rotating body	0.18 - 0.55 % ($k = 2$)

mixtures. The measurements were carried out in the vapor and supercritical phases for three mixtures with CO_2 mole fraction 0.25, 0.5 and 0.75, between 253 K and 473 K. The data from this reference, which were measured using the same equipment as in our work, is quite reliable. An expanded combined relative uncertainty ($k = 2$) 0.55% is estimated. However, the available data for mixtures with CO_2 mole fraction above 0.75 are still scarce.

The aim of the present study is to provide new experimental data on the viscosity of CO_2 binary mixtures. Binary mixture data are essential in the development of multi-component models. In addition, knowledge on the impact of undesirable components on the viscosity of CO_2 streams can contribute to finding the optimized impurity level with respect to the cost of purification.

In this work, new accurate viscosity data for three binary mixtures, CH07 (0.93 CO_2 + 0.07 H_2), CH20 (0.80 CO_2 + 0.20 H_2), and CN10 (0.90 CO_2 + 0.10 N_2) were measured at four isotherms (273, 298, 323, and 473) K in the gas and superheated gas phases. The measurements were carried out using two rotating body type viscometers available at the thermodynamics laboratory of Ruhr University Bochum (RUB). The experimental data are also compared to the data estimated from the extended corresponding states (ECS) model [27] implemented in the NIST Reference Fluid Thermodynamic and Transport Properties (REFPROP 10.0) database [28,29]. In this article, the experimental method is described in Section 2. In Section 3, the uncertainty analysis is provided, experimental results are presented and discussed, and conclusions are drawn in Section 4.

2. Experimental methods

2.1. Apparatus description

More detailed description of the apparatuses used in this work is presented in References [21,30–32]. The general principles are given here. Two rotating body viscometers were utilized, both of which can be operated independently of each other. The low-pressure viscometer (LPV) is designed for low pressures up to 2.0 MPa [32]. At higher pressures up to 20 MPa, a combined viscometer-densimeter or high-pressure viscometer (HPV) is used [31,32]. The viscometer-densimeter integrates a single-sinker densimeter and a rotating-body viscometer. No density measurements were carried out in the present work since highly accurate models for the calculation of density at given pressure, temperature and composition are available [33]. Uncertainties in density measurements would be higher than the uncertainty of the models. Schematics of both viscometers are provided in Fig. 1 and Fig. 2.

The basic measuring principle of both viscometers is to quantify the deceleration of the rotation of a vertically levitating slender cylinder, the so-called rotating body, due to the viscous drag of the surrounding fluid. The rotating body is suspended inside the measuring cell by a magnetic suspension coupling. The rotating body is accelerated around the vertical axis by inducing a magnetic field. The magnetic field is produced by four driving coils placed in the outer wall of the measuring cell. When reaching a given rotational speed, the current to these driving coils is switched off. In the presence of fluid in the measuring cell, the speed of the rotating body is decelerated due to the fluid friction. The rotational frequency of rotating body is detected by rotational speed sensors. The damping-constant D used for the viscosity calculation is determined using an exponential function

$$\boldsymbol{n}(\boldsymbol{t}) = \boldsymbol{n}_{\infty}[1 - \mathbf{exp}(-\boldsymbol{Dt})] \tag{1}$$

where n is the number of rotations as a function of time. The damping-constant D and n_∞ are determined by fitting Eq. (1) to the measured (n, t) data points.

In order to cancel out systematic errors due to inaccuracies arising from the geometry of the system and to decrease the uncertainty of measurements, a viscosity ratio approach is applied and helium is used as a reference fluid [34]. The working equation of the viscometers is given by:

$$\eta = \frac{zD - D_R}{D^0_{He} - D_R}\frac{C^0_{He}}{C}\eta^0_{He}, \tag{2}$$

where η is the viscosity of the fluid. The non-stationary parameter z accounts for the non-stationarity of the fluid flow and it can be interpreted as an increase of the axial moment of inertia of the rotating body. The non-stationary parameter depends on the density of the fluid and on the geometry of the measuring cell. The residual damping, D_R, is caused by inhomogeneities in the magnetic field by the permanent magnet, located at the top of the rotating body. Due to these inhomogeneities, eddy currents are induced in the electrical conducting surroundings,

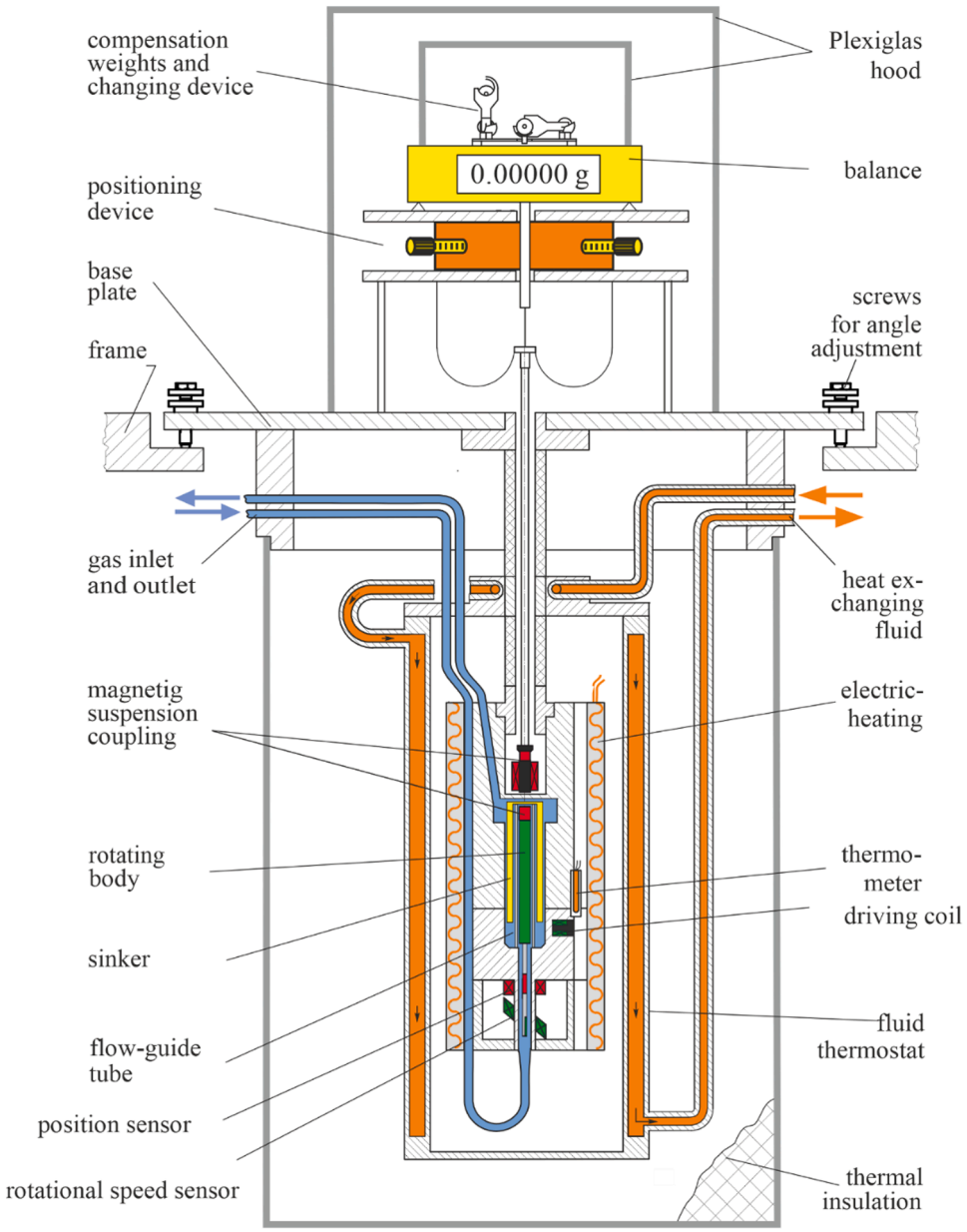

Fig. 1. Schematic of the viscometer-densimeter or high-pressure viscometer [30].

which contribute to an extra damping. The temperature dependent residual damping can be experimentally determined by damping measurements in the evacuated measuring cell. The η^0_{He} is the zero-density viscosity of helium. Here, highly accurate viscosity values calculated from *ab initio* (quantum mechanics and statistical mechanics) with an uncertainty less than 0.001% are used [35]. The D^0_{He} is the damping value of helium at zero density. Since measuring at zero density is not feasible, experimental damping values for helium at low pressures were extrapolated linearly down to zero density. The ${C_{He}}^0$ and C are the apparatus coefficients for He and the sample fluid under test, respectively. These coefficients can be determined by

$$C = \frac{c_{visc}}{J}, \tag{3}$$

$$J = \frac{1}{2} m r_i^2, \tag{4}$$

where J is the axial moment of inertia of the rotating body. m and r_i are the mass and dimeter of rotating body, respectively, and c_{visc} is a collective viscous coefficient. Indeed, c_{visc} combines two different fluid flow regions occurring in the measurement cell during rotation of the rotating body. The disk flow on top and on the bottom of the rotating body and the cylindrical Couette flow in the gap between the rotating body and the flow-guide tube. Both disk and Couette flows depend on the information of dimensions and mass of the measuring cell, rotating body and sensor rod as well as Reynolds number. They are only considered for the high-pressure viscometer, where the apparatus coefficient becomes dependent on the Reynolds number [21].

Precise temperature control is important because the viscosity dependence on temperature is significant. A two-stage thermostat and proper thermal insulation were implemented for precise temperature control. A flow thermostat (Huber thermostatic bath; type 510w) with a double wall stainless-steel container was used as an outer stage. The inner stage includes an electrical heating device attached to the measuring cells. Temperature controllers (Fluke calibration, type 2100 and Fluke calibration, type 2200) were installed for the high-pressure and the low-pressure viscometers, respectively. A 25 Ω standard platinum resistance thermometer (SPRT) (Isotech, type:909) in the low-

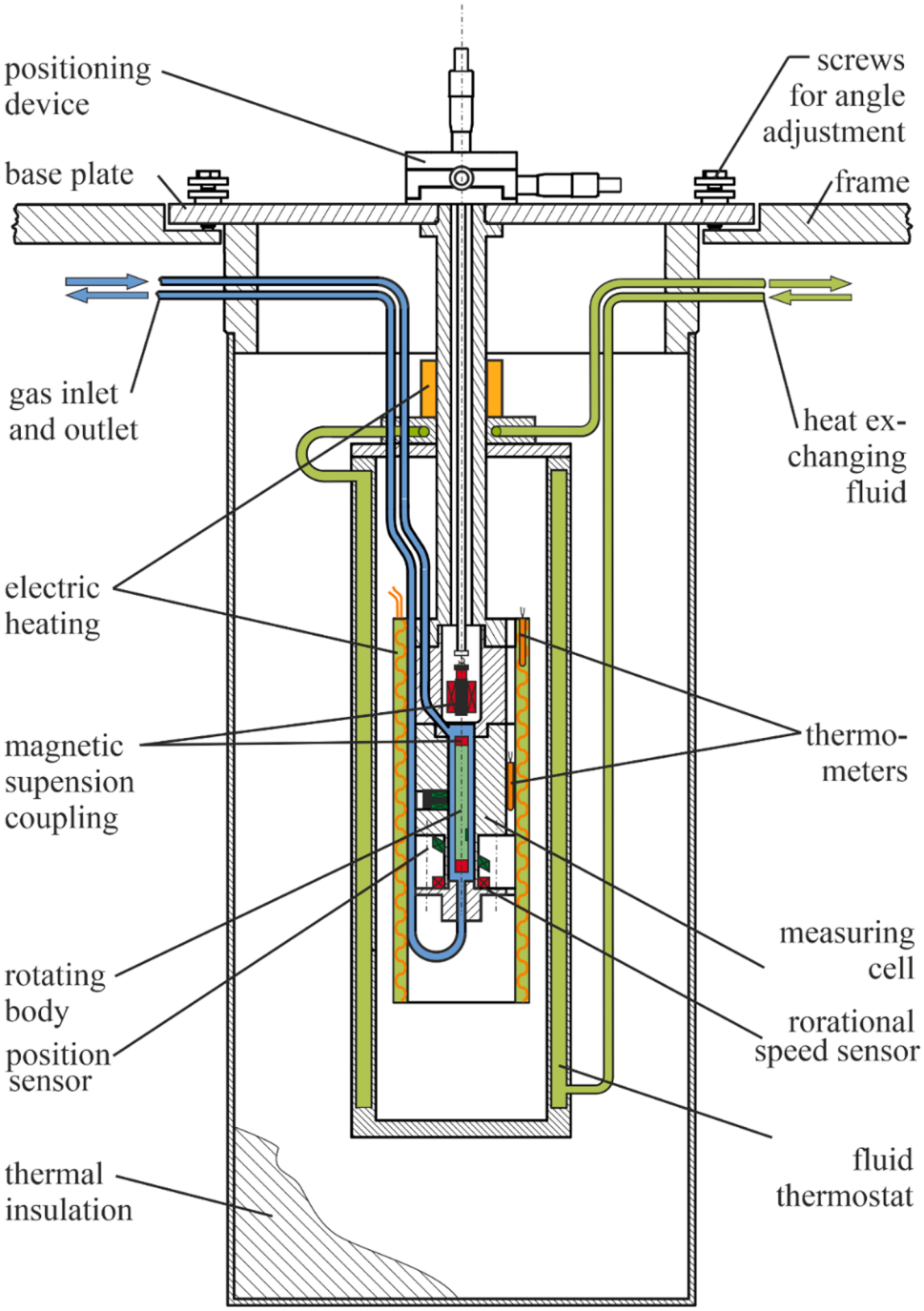

Fig. 2. Schematic of the low-pressure viscometer [30].

pressure viscometer and a Pt-100 Ω sensor (Merz, Germany, type: P100/2528) in the high-pressure viscometer are in direct contact with the measuring cell for the temperature measurement. In addition, a Pt-100 Ω sensor (Merz, Germany, type: P100/2528) was installed in each viscometer for temperature control purposes. All sensors were calibrated according to the temperature calibration standard ITS-90 (International Temperature Scale of 1990 [36]) and .an uncertainty of 50 mK for the high-pressure viscometer and 162 mK for the low- pressure viscometer were reported.

For the pressure measurement of the low- pressure viscometer, a vibrating quartz crystal type pressure transmitter (Paroscientific, type 1500A-01) with a full-scale pressure of 3.45 MPa was used and calibrated against a highly accurate rotating-piston gauge (Fluke Calibration, type PG7601) up to a pressure of 2.1 MPa. For the pressure measurements of the high-pressure viscometer, a sensor with a full-scale pressure of 41.68 MPa (Paroscientific, type 1006 K-01) was used, calibrated with another rotating piston gauge (Desranges and Huot, type DPG5). The uncertainties of the pressure sensors used in the high pressure and low-pressure viscometers are 0.0042 MPa and 0.00035 MPa, respectively.

2.2. *Experimental material*

The three investigated binary mixtures were prepared gravimetrically according to the metrological standards [37] for mixture preparation. A customized setup described in [32] was used. Pure components used for the mixture preparation are listed with information on suppliers and purity in Table 3. The final mixture compositions and the expanded

Table 3
Pure fluids used in the experiments.

Chemical	Source	Final mole fraction purity
CO_2	Air Products, Germany	0.999995[a]
H_2	Air Liquide, Germany	0.999990[b]
N_2	Air Liquide, Germany	0.999990[c]
He	Air Liquide, Germany	0.999999[d]

No additional purification was done.
Impurities reported by suppliers:
[a] $x_{(CO)} < 0.5\bullet10^{-6}$; $x_{(H2O)} < 2.0\bullet10^{-6}$; $x_{(O2)} < 0.5\bullet10^{-6}$; $x_{(N2)} < 2.0\bullet10^{-6}$; $x_{(CnHm)} < 0.1\bullet10^{-6}$
[b] $x_{(CO)} < 0.1\bullet10^{-6}$; $x_{(CO2)} < 0.1\bullet10^{-6}$; $x_{(H2O)} < 2.0\bullet10^{-6}$; $x_{(O2)} < 2.0\bullet10^{-6}$; $x_{(N2)} < 5.0\bullet10^{-6}$; $x_{(CnHm)} < 0.1\bullet10^{-6}$
[c] $x_{(H2O)} < 2.0\bullet10^{-6}$; $x_{(O2)} < 2.0\bullet10^{-6}$; $x_{(CnHm)} < 0.2\bullet10^{-6}$
[d] $x_{(H2O)} < 0.5\bullet10^{-6}$; $x_{(O2)} < 0.1\bullet10^{-6}$; $x_{(CO)} < 0.1\bullet10^{-6}$; $x_{(H2)} < 0.1\bullet10^{-6}$; $x_{(CO2)} < 0.1\bullet10^{-6}$; $x_{(CnHm)} < 0.1\bullet10^{-6}$

Table 4
Mole fractions x and expanded uncertainties in composition $U(x)$ of each mixture ($k = 2$).

Mixture (Component 1 + Component 2)	$x_{component\ 1}$	$x_{component\ 2}$	$U(x)$ $(k=2)$
CH20 ($CO_2 + H_2$)	0.80087	0.19912	$7.0\bullet10^{-5}$
CH07 ($CO_2 + H_2$)	0.93236	0.06763	$1.5\bullet10^{-4}$
CN10 ($CO_2 + N_2$)	0.89980	0.10020	$7.5\bullet10^{-5}$

uncertainties of each binary mixture are reported in Table 4. The mixtures were prepared and kept in aluminum cylinders with a volume of 20 L. The cylinders were supplied with special treated interior surfaces (Aculife inerting, Scott Specialty Gases) for long-term stability of the mixture compositions.

2.3. Experimental procedure

The validity of the model function introduced in Eq. (2) strongly depends on the concentric alignment of the rotating body in the measuring cell. The concentric alignment was performed at each isotherm for the high-pressure viscometer to minimize the uncertainty of the position of the rotating body. The concentric alignment of the rotating body was adjusted using micrometer screws with a resolution of 10 μm. With these micrometer screws, the electromagnet was moved in x, y and z axes and damping values were checked. The minimum damping value is corresponding to the concentric alignment and the most stable position of the rotating body. For this purpose, damping of helium at the pressure of 0.2 MPa were regularly checked. However, for the low-pressure viscometer the centering was quite stable over time and minor changes in the damping values were observed. The viscosity measurements were carried out at four isotherms with a sequence of temperatures (298, 323, 473 and 273) K and again back to 298 K to check the reproducibility. At each isotherm, measurements were started with the following filling procedure: 1) empty the measuring cell to atmospheric pressure, 2) evacuate the measuring cell using a rotary-vane pump (Oerlikon Leybold Vakuum, Germany, type: TRIVAC D 2,5 E) and a turbo molecular pump (Oerlikon Leybold Vakuum, Germany,

Table 5
Budget for the expanded combined uncertainty in viscosity at $T = 298$ K and $p = 0.417$ MPa for the mixture CN10 using the high-pressure viscometer.

Source of uncertainty (f)	Uncertainty	Distribution	Coverage factor	Sensitivity coefficient $\partial\eta/\partial f$	Standard uncertainty u/μPa. s
Viscosity (η)	0.07 μPa.s	Normal	2	1	0.03
Pressure (p)	0.004 MPa	Rectangular	1.73	0.048	0.0003
Temperature (T)	50 mK	Rectangular	1.73	0.132	0.0014
Composition (x_{CO2})	0.00004 mol/mol	Rectangular	1.73	3.258	0.00008
Combined expanded uncertainty U_c ($k = 2$)	0.07 μPa . s				

Table 6
Budget for the uncertainty in viscosity $u(\eta)$ at $T = 298$ K and $p = 0.417$ MPa for the mixture CN10 using the high-pressure viscometer.

Source of uncertainty f	Uncertainty	Distribution	Coverage factor	Sensitivity coefficient $\partial\eta/\partial f$	Standard uncertainty u/μPa. s
Damping of sample fluid (D)	13 μHz	Normal	2	0.00421	0.03
Damping of helium at zero density (D^0_{He})	12 μHz	Rectangular	1.73	0.00323	0.02
Residual damping (D_R)	10 μHz	Rectangular	1.73	0.00097	0.006
Other contributions					0.00016
Expanded uncertainty ($k = 2$)	0.07 μPa .s				

Table 7
Budget for the uncertainty of the damping D at $T = 298$ K and $p = 0.417$ MPa for the mixture CN10 using the high-pressure viscometer.

Source of uncertainty f	Uncertainty/μHz	Distribution	Coverage factor	Sensitivity coefficient $\partial\eta/\partial f$	Standard uncertainty u/μPa. s
Regression	0.3	Rectangular	1.73	1	0.16
Scatter	0.8	Normal	2	1	0.4
Sorption	10	Rectangular	1.73	1	6
Eccentric alignment	5	Rectangular	1.73	1	3
Expanded uncertainty ($k = 2$)	13				

Table 8
Budget for the uncertainty of the damping D^0_{He} at T= 298 K and p= 0.417 MPa for the mixture CN10 using the high-pressure viscometer.

Source of uncertainty f	Uncertainty/μHz	Distribution	Coverage factor	Sensitivity coefficient $\partial\eta/\partial f$	Standard uncertainty u/ μPa. s
Regression	0.6	Rectangular	1.73	1	0.4
Scatter	6	Normal	2	1	3
Eccentric alignment	9	Rectangular	1.73	1	0.8
Extrapolation to the zero density	1.3	Rectangular	1.73	1	5
Expanded uncertainty ($k = 2$)	12				

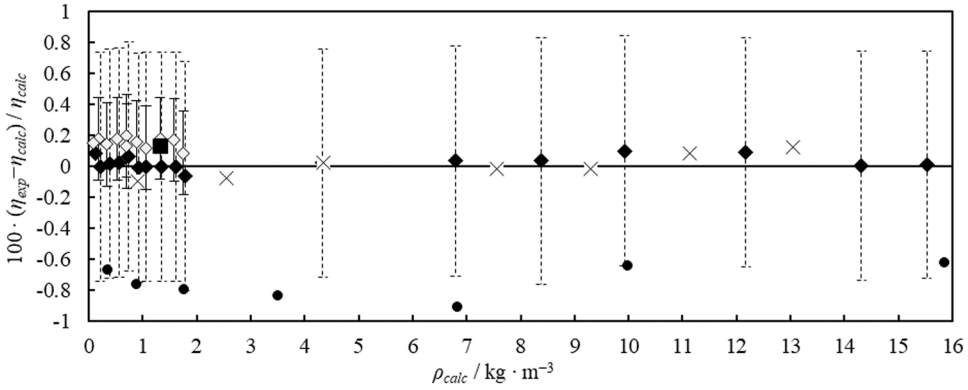

Fig. 3. Relative deviations of experimental viscosities η_{exp} from calculated viscosities η_{calc} for pure hydrogen at $T = 273$ K. ρ_{calc} and η_{calc} are density and viscosity calculated from models [42] and [44], respectively, implemented in NIST REFPROP 10.0 [28, 29]. This work – HPV (◆); this work – LPV (◇); Golubev and Petrovl (1959) [15] (■); Barua et al. (1964) [43] (×); Chuang et al. (1976) [45] (●). The dashed and solid vertical apparent error bars are corresponding to the expanded combined relative uncertainty using high-pressure and low-pressure viscometers, respectively.

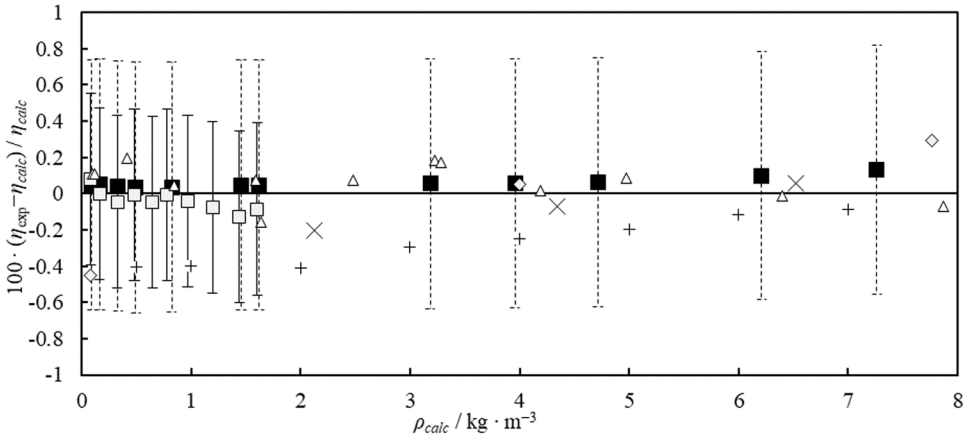

Fig. 4. Relative deviations of experimental viscosities η_{exp} from calculated viscosities η_{calc} for pure hydrogen at $T = 298$ K. ρ_{calc} and η_{calc} are the viscosity and density calculated from models [42] and [44], respectively, implemented in NIST REFPROP 10.0 [28,29]. This work – HPV (■); this work – LPV (□); Barua et al. (1964) [43] (×); Golubev and Petrov (1959) [15] (◇); Gracki et al. (1969) [46] (+); Hongo and Iwasaki (1978) [47] (Δ). The dashed and solid vertical apparent error bars are corresponding to the expanded combined relative uncertainty using high-pressure and low-pressure viscometers, respectively.

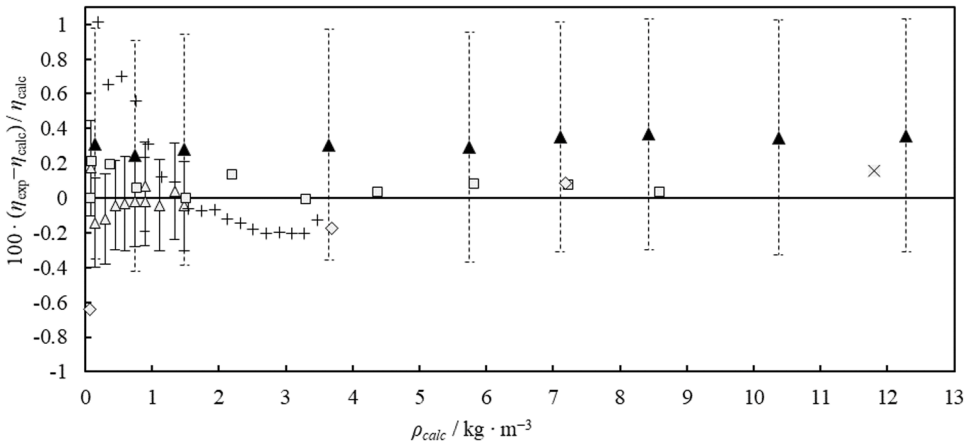

Fig. 5. Relative deviations of experimental viscosities η_{exp} from calculated viscosities η_{calc} for pure hydrogen at $T = 323$ K. ρ_{calc} and η_{calc} are the viscosity and density calculated from models [42] and [44], respectively, implemented in NIST REFPROP 10.0 [28, 29]. This work – HPV (▲); This work – LPV (Δ); Michels et al. (1953) [48] (×); Golubev and Petrov (1959) [15] (◇); Hongo and Iwasaki (1978) [47] (□); Nabizadeh and Mayinger (1999) [49] (+). The dashed and solid vertical apparent error bars are corresponding to the expanded combined relative uncertainty using high-pressure and low-pressure viscometers, respectively.

type: TURBOVAC 50) for 15 minutes, 3) refill the measuring cell with the sample fluid to 0.2 MPa, 4) evacuate for 15 minutes again and repeat steps 3 and 4 at least three times. Meanwhile damping values were recorded after each refilling. When no change in the damping values was observed, the measuring cell was filled up with the sample fluid. The system was pressurized to a pressure restricted by the phase boundary and the state of the flow. In order to avoid condensation of fluid during the measurements filling, the tubing from the gas cylinder to the thermostated measurement cells was temperature-controlled by an electric heating wire. For all measurements, the tubing temperature was set to 323.15 K, which is far above the critical temperature of CO_2 (304.13). The phase boundary of test fluid was also investigated before each measurement and a margin of at least 0.5 MPa were considered to keep the fluid in the gas or supercritical gas phases inside the measuring cell. The flow model is only valid, if a laminar flow is established around the cylinder. To avoid the occurrence of so-called Taylor-vortices, the maximum rotational frequency is limited by the so-called Taylor number *Ta* [38], which is a Reynolds number equivalent for the cylindrical flow. The Taylor number is calculated by

$$Ta = \frac{2\delta^2 d^4}{1-\delta^2} \cdot \frac{(2\pi f)^2 \rho^2}{\eta^2}, \tag{5}$$

where δ is the ratio of the inner and outer radius and d is the difference between outer and inner radius. Values for density and viscosity were

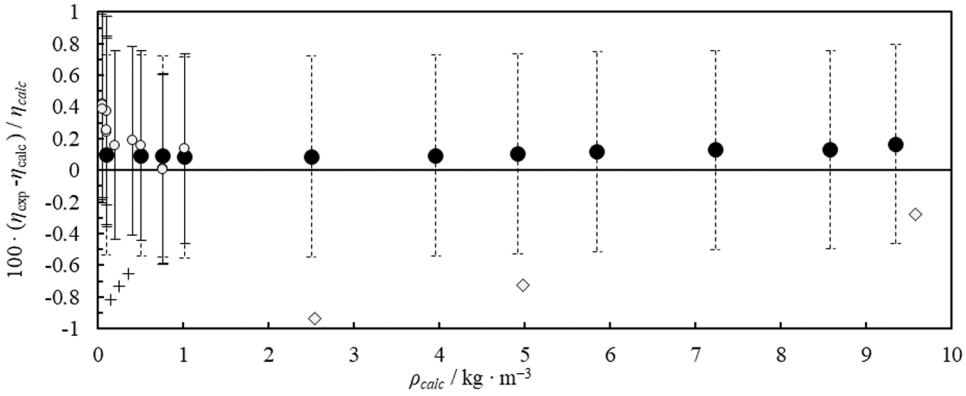

Fig. 6. Relative deviations of experimental viscosities η_{exp} from calculated viscosities η_{calc} for pure hydrogen at $T = 473$ K. ρ_{calc} and η_{calc} are the viscosity and density calculated from models [42] and [44], respectively, implemented in NIST REFPROP 10.0 [28,29]. This work – HPV (●); this work – LPV (○); Golubev and Petrov (1959) [15] (◊); Sakado et al. (2015) [50] (+). The dashed and solid vertical apparent error bars are corresponding to the expanded combined relative uncertainty using high-pressure and low-pressure viscometers, respectively

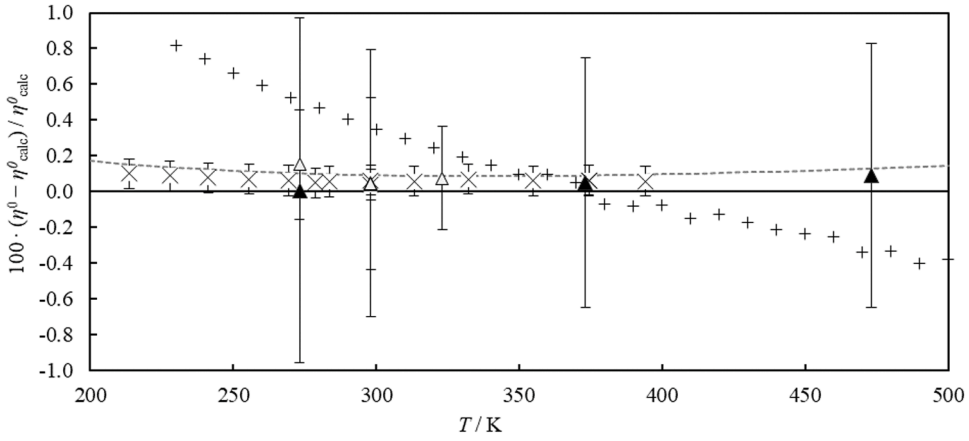

Fig. 7. Relative deviations of zero-density viscosity values for pure hydrogen as a function of temperature. Experimental values η^0 are compared with calculated values $\eta^{\circ}{}_{calc}$ using the model [44], implemented in NIST REFPROP 10.0 [28,29]. Extrapolated η^0 of this work – HPV (▲); Extrapolated η^0 of this work – LPV (Δ); Assael et al. (1986) [53] (+); May et al. (2007) [52] (×). The dashed line corresponds to the *ab initio* calculation by Mehl et. al (2010) [51].

calculated using the models by Refs. [27,28] as implemented in REFPROP 10.0 [29]. Frequency and pressure were chosen in a way, that the actual Taylor number did not exceed the critical Taylor number Ta_{crit}, which was calculated according to

$$\boldsymbol{Ta_{crit}} = 1666.5 \cdot \boldsymbol{\delta}^{-0.8682}. \quad (6)$$

The measurements with the low-pressure viscometer were additionally restricted by the Reynolds number *Re* of the disk flow. For $Re < 30$, the working equation (2) becomes independent from the apparatus coefficients. Thus, frequency and pressure were chosen in a way, that the Reynolds number did not exceed 30. The Taylor criterion is always fulfilled, if $Re < 30$. The cylinder with the sample fluid was heated up using an electrical heating jacket one hour before starting the measurement. Heating the sample fluid at the bottom causes convection inside the cylinder to get a homogenization of the mixture.

According to Eq. (2), precise knowledge of three parameters D, D^0_{He} and D_R is necessary to calculate the experimental viscosity. The damping values D of the fluids under test were measured at each isotherm and desired pressure point. For this purpose, the rotating body was first accelerated using the drive coils until they switched off at a given maximum rotational frequency f_{max}, after which the rotating body decelerated mainly due to fluid friction. The values of f_{max} were set such that the flow around the rotating body remained laminar. For each data point, this measurement of D values was repeated five times, and an average value was used for the viscosity measurements. In order to determine the zero-density damping value of helium, D^0_{He}, the damping of helium was measured at pressures from 0.1 to 1 MPa at each temperature. To determine D^0_{He}, these measurements were extrapolated to zero-density using a linear fit. To determine the experimental residual damping value, D_R, at each isotherm, the measurement cell was evacuated down to a vacuum pressure $< 5 \bullet 10^{-3}$ Pa, requiring a two-stage evacuation. A rotary-vane pump (Oerlikon Leybold Vakuum, Germany, type: TRIVAC D 2,5 E) was used to reach 4.0 Pa within a few minutes, followed by a turbo-molecular pump (Oerlikon Leybold Vakuum, Germany, type: TURBOVAC 50) which reached a high level of vacuum pressure of 1•10−3 Pa within a few days, after which damping measurements were carried out. D_R was determined by extrapolating the measured damping values to zero-pressure using a linear fit. Although D_R was measured under ultra-high vacuum pressure, extrapolating the measured damping values to zero-pressure using a linear fit is necessary. The reason for that is residual damping is one of the main contributions to the uncertainty of measurement and the effect of viscosity at even very low pressures cannot be neglected.

3. Results and discussion

3.1. Uncertainty analysis

The uncertainty analysis was conducted based on the guide to the expression of uncertainty in measurement [39]; the main contributions to uncertainty introduced by [40] apply for this work as well. The overall combined standard uncertainty for the viscosity measurements U_c (η (*T*,*p*,*x*)) is determined from:

Table 9
Experimental dynamic viscosity data for the binary mixture CH07, where T is the temperature, p is the pressure, ρ_{calc} is the density calculated from [54] implemented in the thermodynamic software tool, Trend 5.0 [55], η_{exp} is the dynamic experimental viscosity data, η_{calc} is the viscosity calculated using the Extended Corresponding States (ECS) model [27] implemented in NIST REFPROP 10.0 [28,29] and $U_c(\eta)$ is the expanded combined uncertainty ($k = 2$) in viscosity. $U_r(\eta)$ is the expanded combined relative uncertainty ($k = 2$) in viscosity.

T / K	p / MPa	ρ_{calc} / kg. m^{-3}	η_{exp} / μPa•s	$U_c(\eta)$ / μPa•s (k = 2)	100 × $U_r(\eta)$ (k = 2)	100 × (η_{exp}-η_{calc})/η_{calc}
High-pressure viscometer						
273.16	3.468	84.919	14.400	0.078	0.543	-0.548
273.15	2.991	69.350	14.200	0.086	0.606	-0.484
273.15	2.502	55.307	14.062	0.075	0.533	-0.390
273.15	1.985	42.020	13.907	0.072	0.521	-0.380
273.16	1.780	37.098	13.881	0.075	0.542	-0.295
273.16	1.502	30.712	13.850	0.077	0.555	-0.130
273.16	1.182	23.715	13.820	0.075	0.544	0.048
273.16	0.972	19.307	13.795	0.072	0.522	0.095
273.15	0.773	15.253	13.787	0.072	0.519	0.235
273.15	0.581	11.443	13.77	0.068	0.490	0.335
273.15	0.391	7.773	13.766	0.068	0.492	0.401
273.15	0.190	3.970	13.748	0.069	0.500	0.422
298.15	4.659	101.179	16.078	0.075	0.463	-0.121
298.15	4.014	83.920	15.754	0.074	0.470	-0.232
298.15	3.010	58.388	15.399	0.073	0.474	-0.235
298.16	2.009	46.738	15.174	0.071	0.468	-0.244
298.15	1.808	32.812	15.138	0.071	0.469	-0.012
298.16	1.507	26.924	15.093	0.071	0.469	0.069
298.15	1.204	21.177	15.04	0.071	0.470	0.119
298.16	1.013	17.651	15.029	0.071	0.471	0.201
298.15	0.811	13.991	15.009	0.066	0.442	0.269
298.15	0.601	10.267	14.989	0.066	0.442	0.337
298.15	0.207	3.473	14.95	0.066	0.443	0.468
323.15	4.512	82.785	17.139	0.075	0.439	-0.260
323.15	3.995	71.550	16.907	0.074	0.440	-0.244
323.15	2.985	51.152	16.609	0.073	0.442	-0.121
323.15	2.017	33.252	16.406	0.073	0.442	0.029
323.15	1.805	29.509	16.370	0.073	0.443	0.064
323.15	1.505	24.342	16.319	0.072	0.443	0.088
323.15	1.203	19.232	16.274	0.068	0.416	0.125
323.15	1.003	15.924	16.253	0.067	0.414	0.188
323.15	0.819	12.925	16.225	0.067	0.414	0.185
323.15	0.602	9.430	16.196	0.067	0.415	0.189
323.15	0.403	6.267	16.170	0.076	0.470	0.189
473.15	6.005	65.673	23.794	0.091	0.383	0.531
473.15	6.005	65.668	23.793	0.089	0.372	0.528
473.15	5.006	54.373	23.591	0.089	0.375	0.472
473.15	5.007	54.388	23.593	0.088	0.373	0.482
473.15	4.002	43.155	23.390	0.088	0.375	0.380
473.15	3.011	32.238	23.226	0.079	0.341	0.384
473.15	2.001	21.264	23.069	0.079	0.342	0.391
473.15	1.505	15.935	22.987	0.079	0.343	0.356
473.15	1.001	10.560	22.919	0.079	0.344	0.374
473.15	0.816	8.599	22.893	0.079	0.344	0.376
473.15	0.608	6.398	22.866	0.079	0.345	0.384
473.15	0.403	4.231	22.847	0.079	0.345	0.425
473.15	0.200	2.106	22.829	0.079	0.345	0.468
Reproducibility check						
298.15	4.533	98.275	16.039	0.077	0.478	0.047
298.15	4.213	89.069	15.890	0.076	0.481	0.084
298.15	4.008	83.447	15.798	0.076	0.484	0.062
298.15	3.515	70.670	15.590	0.076	0.485	-0.051
298.15	2.506	47.298	15.266	0.075	0.489	-0.205
298.15	2.009	36.864	15.163	0.074	0.491	-0.126
298.15	1.511	26.991	15.088	0.073	0.484	0.030
298.15	0.993	17.291	15.026	0.073	0.485	0.200
Low-pressure viscometer						
273.15	0.602	11.339	13.781	0.032	0.234	0.367
273.15	0.400	7.445	13.765	0.033	0.236	0.414
273.14	0.206	3.781	13.761	0.032	0.234	0.526
273.14	0.104	1.903	13.759	0.032	0.232	0.580
298.14	0.604	10.313	14.974	0.037	0.244	0.053
298.14	0.403	6.819	14.953	0.038	0.251	0.058
298.14	0.202	3.393	14.934	0.037	0.248	0.072
298.14	0.101	1.692	14.932	0.036	0.243	0.126
323.15	0.802	12.641	16.203	0.034	0.211	0.062
323.15	0.599	9.385	16.169	0.035	0.218	0.026
323.16	0.402	6.260	16.154	0.033	0.207	0.090
323.15	0.202	3.122	16.136	0.034	0.209	0.128
323.15	0.104	1.599	16.124	0.034	0.208	0.125
473.15	1.267	12.674	22.934	0.042	0.184	0.318
473.15	1.062	10.624	22.901	0.048	0.209	0.291
473.15	0.845	8.452	22.872	0.053	0.230	0.292
473.15	0.638	6.383	22.842	0.044	0.193	0.280
473.15	0.425	4.259	22.821	0.043	0.188	0.310
473.15	0.213	2.131	22.792	0.043	0.188	0.302
473.14	0.110	1.105	22.784	0.045	0.195	0.326
Reproducibility check						
298.15	0.805	13.881	14.982	0.037	298.15	0.805
298.15	0.609	10.415	14.968	0.033	298.15	0.609
298.15	0.401	6.793	14.955	0.036	298.15	0.401

$$u_c(\eta\ (\boldsymbol{T},\boldsymbol{p},\boldsymbol{x})) = \sqrt{\boldsymbol{u}\ (\eta)^2 + \left[(\partial\eta/\partial\boldsymbol{T})_{p,x}\boldsymbol{u}(\boldsymbol{T})\right]^2 + \left[(\partial\eta/\partial\boldsymbol{p})_{T,x}\boldsymbol{u}(\boldsymbol{P})\right]^2 + \left[(\partial\eta/\partial\boldsymbol{x})_{T,p}\boldsymbol{u}(\boldsymbol{x})\right]^2} \quad (7)$$

where $u(\eta)$, $u(T)$, $u(p)$ and $u(x)$ are the standard uncertainties of the viscosity, temperature, pressure, and composition, respectively. The uncertainty of the temperature $u(T)$ was determined from the temperature calibration based on the ITS-90 with a maximum value of 50 mK for the high-pressure viscometer and 162 mK for the low- pressure viscometer. The temperature uniformity for both sensors are also included in the uncertainty estimations. The expanded uncertainty (k =1.73) of the temperature measurement was dominated by the temperature gradient along the measuring cell and was estimated to be 104 mK at $T = 253.15$ K increasing to 162 mK at $T = 473.15$ K for the low-pressure viscometer. Temperature gradients along the measuring cell of the high-pressure viscometer did not exceed 30 mK. A temperature stability of 10 mK was achieved during the viscosity measurements. The pressure uncertainties $u(p)$ of 0.0042 MPa and 0.00035 MPa were reported by the manufacturer for the pressure sensors used in the high pressure and low-pressure viscometers, respectively. The high accuracy of pressure sensors was checked regularly by pressure calibration using rotating-piston gauges, as mentioned in section 2.1. The uncertainties in the mixture compositions $u(x)$ are reported in Table 4. The weighing of each component during the mixture preparation were repeated 10 times and the results as well as the zero-point drift of the balance were averaged for each weighing repetition. In order to compensate for the air buoyancy of the cylinders, the air conditions (pressure, temperature and the relative humidity) were measured during the weighing. The sensitivity coefficients in Eq. (7) were estimated using the Extended Corresponding States (ECS) model [25] implemented in NIST REFPROP 10.0 [26,27]. Table 5 presents an example for the expanded combined uncertainty budget at a temperature of 298 K and a pressure of 0.417 MPa for the mixture CN10 using the high-pressure viscometer. The same approach was applied for the low-pressure viscometer as described in [41]; however, the uncertainty was expanded to take into account hysteresis effects in the uncertainty of the damping, which was seen during the measurements.

The main contribution to the expanded combined uncertainty is the uncertainty from the viscosity measurements $u(\eta)$. The main contributions to $u(\eta)$ are the measurement of the damping in the sample fluid D, the residual damping D_R and the damping value for helium at zero density D^0_{He}. However, several other contributions, such as the non-stationary parameter z, the apparatus geometry coefficients, the thermal expansion coefficients of the materials, the mass of the rotating body, the density of the fluid and the viscosity reference value for helium

Table 10
Experimental dynamic viscosity data for the binary mixture CH20, where T is the temperature, p is the pressure, ρ_{calc} is the density calculated from [54] implemented in the thermodynamic software tool, Trend 5.0 [55], η_{exp} is the dynamic experimental viscosity data, η_{calc} is the viscosity calculated using the Extended Corresponding States (ECS) model [27] implemented in NIST REFPROP 10.0 [28,29] and $U_c(\eta)$ is the expanded combined uncertainty ($k = 2$) in viscosity. $U_r(\eta)$ is the expanded combined relative uncertainty ($k = 2$) in viscosity.

T/ K	p/ MPa	ρ_{calc}/ kg. m^{-3}	η_{exp}/ μPa•s	$U_c(\eta)$/ μPa•s (k = 2)	100 × $U_r(\eta)$ (k = 2)	100 × (η_{exp} - η_{calc})/η_{calc}
High-pressure viscometer						
273.18	4.501	91.757	14.669	0.074	0.507	-0.510
273.15	4.018	79.070	14.472	0.075	0.521	-0.460
273.15	4.019	79.081	14.465	0.074	0.510	-0.507
273.15	3.521	66.975	14.303	0.074	0.515	-0.388
273.15	3.023	55.685	14.176	0.073	0.517	-0.187
273.15	2.521	45.051	14.072	0.073	0.520	0.049
273.15	2.028	35.229	14.003	0.072	0.515	0.396
273.15	1.824	31.333	13.976	0.072	0.512	0.527
273.15	1.496	25.253	13.938	0.071	0.513	0.735
273.15	1.199	19.935	13.914	0.071	0.513	0.970
273.15	1.001	16.481	13.906	0.068	0.488	1.164
273.15	0.796	12.969	13.887	0.068	0.487	1.276
273.15	0.597	9.640	13.872	0.068	0.487	1.401
273.15	0.205	3.252	13.857	0.068	0.488	1.713
298.15	5.036	88.139	15.989	0.077	0.479	0.171
298.15	4.054	67.937	15.664	0.076	0.484	0.215
298.15	3.045	48.947	15.423	0.076	0.491	0.462
298.15	2.046	31.632	15.233	0.075	0.491	0.720
298.15	1.842	28.262	15.213	0.073	0.483	0.865
298.15	1.547	23.487	15.173	0.073	0.483	0.984
298.14	1.242	18.645	15.140	0.073	0.484	1.150
298.15	1.039	15.486	15.124	0.071	0.468	1.278
298.16	0.646	9.492	15.088	0.069	0.456	1.479
298.15	0.236	3.417	15.051	0.069	0.456	1.664
323.16	8.742	148.953	18.730	0.083	0.444	1.802
323.16	8.003	133.202	18.334	0.089	0.487	1.582
323.16	7.002	112.972	17.812	0.080	0.451	0.781
323.16	6.007	94.016	17.413	0.079	0.456	0.638
323.16	5.007	76.066	17.086	0.078	0.459	0.597
323.16	2.999	43.038	16.604	0.076	0.457	0.792
323.16	2.008	28.059	16.444	0.073	0.446	1.074
323.16	1.803	25.043	16.418	0.071	0.431	1.160
323.16	1.502	20.696	16.372	0.070	0.430	1.223
323.16	0.991	13.480	16.302	0.070	0.430	1.346
323.16	0.605	8.140	16.262	0.070	0.430	1.499
323.16	0.413	5.527	16.245	0.070	0.431	1.583
323.16	0.211	2.811	16.229	0.070	0.431	1.679
473.15	9.258	87.017	24.255	0.097	0.399	1.859
473.15	9.259	87.020	24.230	0.092	0.380	1.753
473.15	8.046	75.332	23.992	0.092	0.382	1.528
473.16	9.136	85.836	24.205	0.092	0.380	1.741
473.15	8.013	75.015	23.987	0.092	0.382	1.532
473.15	7.010	65.397	23.788	0.092	0.386	1.344
473.15	6.010	55.865	23.611	0.089	0.376	1.283
473.15	5.006	46.364	23.450	0.088	0.377	1.264
473.15	4.005	36.941	23.297	0.088	0.377	1.250
473.15	2.996	27.518	23.168	0.079	0.342	1.321
473.15	2.003	18.319	23.022	0.079	0.343	1.288
473.15	1.230	11.206	22.929	0.079	0.345	1.336
473.15	1.008	9.175	22.904	0.079	0.344	1.351
473.15	0.211	1.913	22.827	0.079	0.344	1.466
Reproducibility checks						
298.15	5.050	88.432	15.968	0.077	298.15	5.050
298.15	2.043	31.582	15.230	0.075	298.15	2.043
298.15	1.027	15.306	15.118	0.070	298.15	1.027
298.15	0.625	9.174	15.075	0.069	298.15	0.625
298.15	0.214	3.103	15.047	0.069	298.15	0.214
Low-pressure viscometer						
273.16	1.013	16.663	13.937	0.036	0.255	1.373
273.15	0.604	9.738	13.891	0.034	0.244	1.529
273.15	0.404	6.449	13.869	0.032	0.234	1.590
273.15	0.207	3.263	13.868	0.032	0.231	1.791
273.16	0.110	1.718	13.862	0.033	0.237	1.845
298.15	0.801	11.841	15.060	0.036	0.242	1.123
298.15	0.604	8.859	15.042	0.038	0.251	1.221
298.15	0.399	5.818	15.015	0.042	0.282	1.258
298.15	0.202	2.922	15.008	0.036	0.243	1.414
298.15	0.104	1.501	15.003	0.037	0.247	1.479
323.15	1.004	13.626	16.282	0.035	0.213	1.214
323.15	0.752	10.864	16.253	0.036	0.220	1.291
323.15	0.602	8.081	16.224	0.034	0.209	1.269
323.15	0.404	5.400	16.202	0.035	0.217	1.322
323.15	0.203	2.698	16.190	0.034	0.209	1.444
323.15	0.103	1.384	16.188	0.035	0.218	1.531
473.15	1.936	17.698	23.014	0.043	0.187	1.354
473.16	1.801	16.458	22.987	0.042	0.184	1.357
473.16	1.502	13.708	22.938	0.042	0.184	1.277
473.16	1.202	10.951	22.904	0.042	0.184	1.306
473.16	0.998	9.089	22.877	0.043	0.187	1.302
473.15	0.802	7.297	22.855	0.043	0.189	1.320
473.16	0.603	5.484	22.838	0.043	0.189	1.360
473.16	0.406	3.688	22.808	0.043	0.187	1.339
473.15	0.206	1.871	22.802	0.042	0.185	1.428
473.16	0.107	0.966	22.784	0.043	0.190	1.402
Reproducibility checks						
298.15	0.801	11.833	15.092	0.036	298.15	0.801
298.15	0.601	8.819	15.070	0.037	298.15	0.601
298.15	0.400	5.829	15.054	0.037	298.15	0.400
298.15	0.202	2.930	15.053	0.037	298.15	0.202
298.15	0.105	1.508	15.042	0.037	298.15	0.105

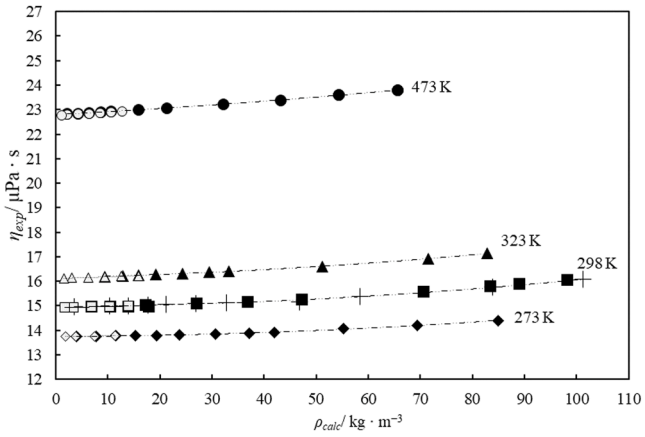

Fig. 8. Dynamic viscosity data for the mixture CH07 are plotted versus the density of the mixture, ρ_{calc} calculated with the improved GERG-2008 model [54] as implemented in the thermodynamic software tool Trend 5.0 [55]. 273 K – HPV (◆); 273 K - LPV (◇); 298 K – HPV (■); 298 K- LPV (□); 323 K – HPV (▲); 323 K – LPV (Δ); 473 K – HPV (●); 473 K – LPV (○); 298 K- reproducibility check (+). The dashed line corresponds to a second-order polynomial fit to the data.

at zero density η^0_{He} also have a small impact on the uncertainty. The sum of all these minor uncertainty contributions is given as 'other contribution' in Table 6.

The uncertainties of D and D^0_{He} provided in Table 6 are combined values. Several sources of uncertainty are included as listed in Table 7 and Table 8. The term 'Regression' refers to the standard deviation of the regression performed to estimate the measured damping values D and $D_{He}{}^{\circ}$ from Eq. (1). Each viscosity value is calculated from an average of five successive measurements (repeatability of measurements) and the uncertainty source of 'scatter' is the standard deviation of the damping values of these five measurements. In order to minimize the influence of sorption, i.e., adsorption/desorption of components in/from the surfaces of tubes and measuring cell, the measurement cell was evacuated and flushed with fresh the test fluid several times after the fluid or temperature was changed. However, a small change in the composition of the

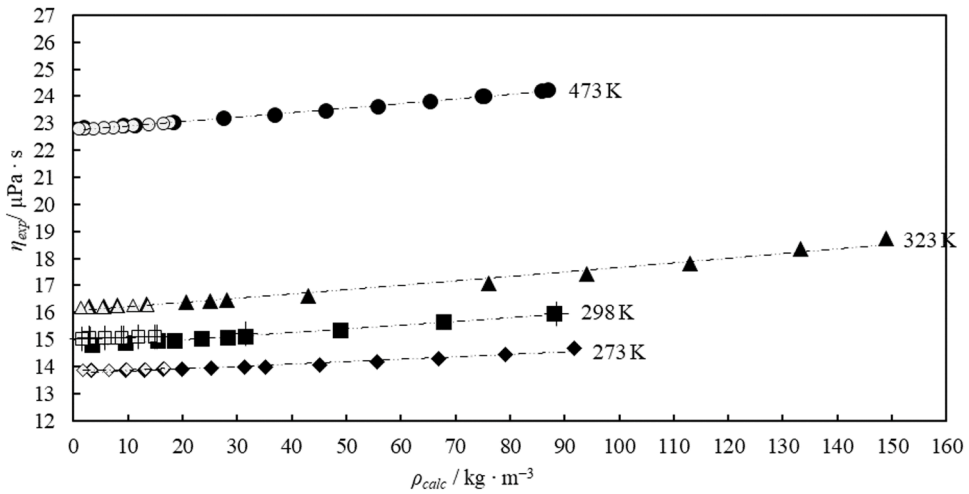

Fig. 9. Dynamic viscosity data for the mixture CH20 are plotted versus the density of the mixture, ρ_{calc} calculated with the improved GERG-2008 model [54] as implemented in the thermodynamic software tool Trend 5.0 [55]. 273 K - HPV (◆); 273 K - LPV (◇); 298 K – HPV (■); 298 K- LPV (□); 323 K – HPV (▲); 323 K – LPV (Δ); 473 K – HPV (●); 473 K – LPV (○); 298 K- reproducibility check (+). The dashed line corresponds to a second-order polynomial fit to the data.

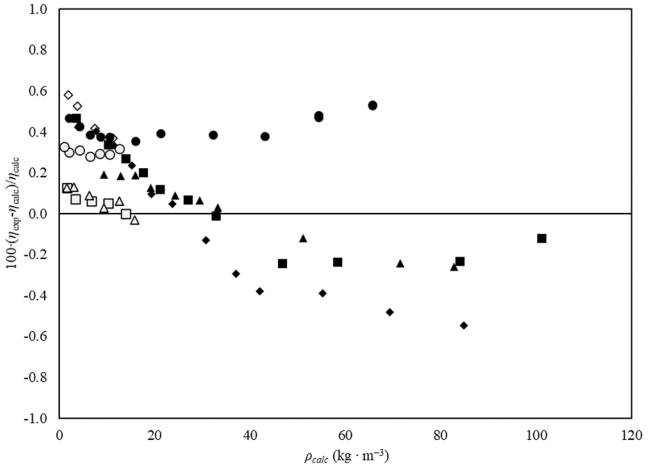

Fig. 10. Relative deviations between experimental and calculated viscosity values, η_{exp} and η_{calc}, for the mixture CH07. η_{calc} is calculated using the Extended Corresponding States (ECS) model [27] implemented in NIST REFPROP 10.0 [28,29]. Deviations are plotted versus density ρ_{calc} calculated with the improved GERG-2008 model [54], implemented in the thermodynamic software tool, Trend 5.0 [55]. 273 K - HPV (◆); 273 K - LPV (◇); 298 K – HPV (■); 298 K- LPV (□); 323 K – HPV (▲); 323 K – LPV (Δ); 473 K – HPV (●); 473 K – LPV (○).

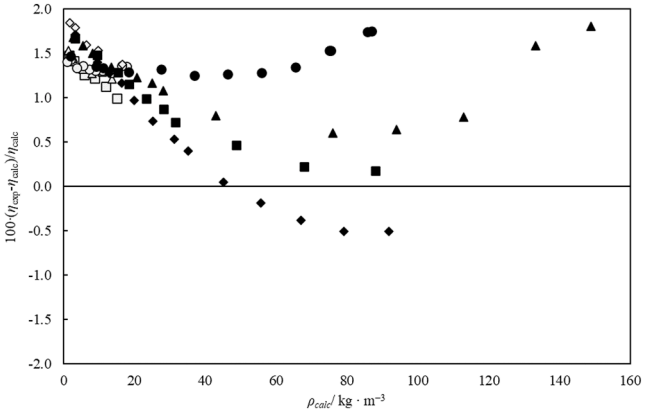

Fig. 11. Relative deviations between experimental, η_{exp}, and calculated, η_{calc}, viscosity values for the mixture CH20 η_{calc} is calculated using the Extended Corresponding States (ECS) model [27] implemented in NIST REFPROP 10.0 [28,29]. Deviations are plotted versus density ρ_{calc} calculated with the improved GERG-2008 model [54], implemented in the thermodynamic software tool Trend 5.0 [55].273 K - HPV (◆); 273 K - LPV (◇); 298 K – HPV (■); 298 K- LPV (□); 323 K – HPV (▲); 323 K – LPV (Δ); 473 K – HPV (●); 473 K – LPV (○).

mixtures due to sorption effects might impact the uncertainty of measurements. Therefore, long-term measurements with a duration of at least 48 hours to check the damping values of gas under test were carried out. During the first few hours, a negligible drift in damping values were observed. However, the results of long-term measurements were considered in the uncertainty estimation. The mixtures with H_2 showed stronger sorption effects than the mixture with N_2 since a larger drift in the damping values was observed for H_2. The small size of H_2 molecules might explain this effect.

3.2. Viscosity validation

The high-pressure viscometer and the low-pressure viscometer have already been validated with pure CO_2 by References [21,40], respectively. Nevertheless, both apparatuses were validated again in this work by measuring the viscosity isotherms of pure hydrogen at (273, 298, 323 and 473) K. Results of the validation measurements are given in Fig. 3. The measured results of this work are compared with the predictions of using the model [41] as implemented in NIST REFPROP 10.0 [26,27]. The deviation between experimental and calculated data plotted versus density. The density of pure hydrogen was calculated from the model of Ref. [42] as implemented in NIST REFPROP 10.0 [28,29]. The experimental data are in a good agreement with the model predictions and the maximum deviation was 0.42%, which is comparable to the estimated experimental uncertainty. Comparisons with existing data were made as well. At a temperature of 273 K, the measured data within this work agree well with the data of Ref. [43], which seems to be the data set, the model has been fitted to. There is an agreement between measured data and existing data at 298 K and 323 K (Figs. 4–6).

The viscosity of any gas can be represented by a virial expansion series

$$\eta(T,\rho) = \eta^0(T) + \eta^1(T)\rho + \eta^2(T)\rho^2 + \cdots \quad (8)$$

By fitting the first three terms of the virial expansion (8) to the measured data, the extrapolated zero-density viscosity η^0 is found. Fig. 7 shows the deviation of extrapolated zero-density viscosities from the

Table 11
Experimental dynamic viscosity data for the mixture CN10, where T is the temperature, p is the pressure, ρ_{calc} is the density calculated from the GERG-2008 EOS [56] implemented in NIST REFPROP 10.0 [28], η_{exp} is the dynamic viscosity data, η_{calc} is the viscosity of Extended Corresponding States (ECS) model [27] implemented in NIST REFPROP 10.0 [28,29] and $U_c(\eta)$ is the expanded combined uncertainty ($k = 2$) in viscosity. $U_r(\eta)$ is the relative combined expanded uncertainty ($k = 2$) in viscosity.

T/ K	p/ MPa	ρ_{calc}/ kg. m^{-3}	η_{exp}/ μPa•s	$U_c(\eta)$/ μPa•s (k = 2)	100 × $U_r(\eta)$ (k = 2)	100 × (η_{exp}-η_{calc})/η_{cac}
High-pressure viscometer						
273.15	3.519	87.987	14.807	0.073	0.490	-0.543
273.15	3.027	71.479	14.555	0.072	0.494	-0.653
273.16	2.510	56.316	14.365	0.071	0.498	-0.676
273.15	2.020	43.410	14.223	0.071	0.500	-0.713
273.16	1.805	38.126	14.178	0.071	0.501	-0.679
273.15	1.506	31.078	14.133	0.071	0.503	-0.558
273.15	1.210	24.437	14.097	0.070	0.495	-0.447
273.15	1.008	20.081	14.074	0.070	0.495	-0.385
273.16	0.802	15.754	14.054	0.070	0.496	-0.322
273.15	0.606	11.747	14.046	0.066	0.468	-0.200
273.16	0.391	7.479	14.027	0.066	0.468	-0.159
273.15	0.215	4.072	14.014	0.066	0.469	-0.121
298.15	5.526	134.482	17.174	0.080	0.464	0.241
298.15	5.011	116.155	16.749	0.079	0.469	0.018
298.15	4.523	100.598	16.430	0.078	0.473	-0.129
298.15	4.012	85.839	16.154	0.077	0.475	-0.271
298.15	3.520	72.747	15.938	0.076	0.479	-0.353
298.15	3.021	60.463	15.774	0.076	0.481	-0.308
298.15	2.510	48.726	15.611	0.075	0.483	-0.402
298.15	2.009	37.922	15.492	0.075	0.486	-0.377
298.15	1.812	33.838	15.453	0.075	0.487	-0.353
298.15	1.515	27.863	15.399	0.074	0.479	-0.315
298.15	1.205	21.816	15.350	0.074	0.480	-0.270
298.15	1.002	17.953	15.329	0.074	0.480	-0.184
298.15	0.811	14.405	15.313	0.069	0.453	-0.098
298.16	0.616	10.848	15.282	0.069	0.452	-0.115
298.15	0.417	7.284	15.255	0.069	0.453	-0.108
298.15	0.811	14.405	15.313	0.069	0.453	-0.098
298.16	0.616	10.848	15.282	0.069	0.452	-0.115
323.15	6.009	122.265	18.285	0.073	0.397	0.531
323.15	5.515	109.285	17.999	0.070	0.387	0.433
323.15	5.008	96.720	17.715	0.069	0.390	0.182
323.15	4.513	85.118	17.502	0.069	0.394	0.138
323.15	3.956	72.710	17.276	0.068	0.396	0.009
323.15	3.519	63.456	17.120	0.068	0.398	-0.082
323.15	3.017	53.262	16.959	0.068	0.400	-0.185
323.15	2.494	43.101	16.825	0.068	0.402	-0.196
323.15	2.020	34.285	16.729	0.067	0.400	-0.131
323.15	1.819	30.631	16.682	0.066	0.395	-0.165
323.15	1.516	25.248	16.628	0.066	0.395	-0.133
323.15	1.201	19.775	16.577	0.066	0.397	-0.099
323.15	1.021	16.693	16.551	0.061	0.367	-0.070
323.15	0.816	13.259	16.520	0.060	0.363	-0.054
323.15	0.614	9.897	16.484	0.060	0.362	-0.081
323.15	0.418	6.698	16.462	0.059	0.360	-0.038
323.15	0.219	3.496	16.433	0.060	0.364	-0.044
473.15	7.291	82.757	24.452	0.093	0.379	0.309
473.15	7.004	79.356	24.383	0.094	0.384	0.282
473.15	6.457	72.900	24.253	0.092	0.380	0.231
473.15	6.001	67.546	24.147	0.092	0.380	0.183
473.15	5.458	61.219	24.022	0.092	0.381	0.116
473.15	5.006	55.973	23.931	0.089	0.373	0.099
473.15	4.505	50.196	23.822	0.089	0.372	0.037
473.15	3.998	44.399	23.715	0.089	0.373	-0.029
473.15	3.506	38.792	23.626	0.088	0.374	-0.044
473.15	3.006	33.146	23.540	0.088	0.374	-0.051
473.15	2.489	27.347	23.458	0.080	0.341	-0.044
473.15	1.996	21.851	23.372	0.079	0.339	-0.080
Reproducibility checks						
298.15	5.521	134.303	17.156	0.080	0.464	0.165
298.15	5.021	116.493	16.751	0.079	0.469	-0.011
298.14	4.532	100.882	16.437	0.078	0.473	-0.115
298.15	4.532	85.965	16.432	0.077	0.469	-0.146
298.15	4.017	72.660	16.175	0.077	0.473	-0.155
298.15	3.516	60.589	15.956	0.076	0.476	-0.236
298.15	3.026	49.084	15.780	0.076	0.479	-0.277
298.15	2.526	40.807	15.606	0.075	0.483	-0.460
298.15	2.146	35.569	15.518	0.075	0.484	-0.416
298.15	1.896	29.564	15.461	0.074	0.480	-0.416
298.15	1.601	23.654	15.415	0.074	0.478	-0.322
298.15	1.300	19.433	15.361	0.074	0.479	-0.303
298.15	1.080	15.679	15.331	0.071	0.462	-0.257
298.15	0.880	12.178	15.313	0.069	0.451	-0.165
298.15	0.689	8.388	15.284	0.069	0.452	-0.167
298.15	0.479	4.880	15.258	0.069	0.453	-0.144
298.15	0.281	1.851	15.242	0.069	0.452	-0.077
298.15	0.107	1.852	15.225	0.069	0.453	-0.053
Low-pressure viscometer						
273.15	0.604	11.706	14.052	0.034	0.243	-0.154
273.15	0.402	7.698	14.019	0.033	0.235	-0.219
273.15	0.20	3.915	14.013	0.035	0.246	-0.126
273.15	0.108	2.037	14.019	0.033	0.239	-0.016
298.15	0.602	10.582	15.240	0.038	0.247	-0.377
298.15	0.400	7.052	15.221	0.037	0.241	-0.325
298.15	0.204	3.536	15.197	0.037	0.241	-0.315
298.15	0.106	1.836	15.187	0.037	0.241	-0.301
323.15	1.00	16.403	16.522	0.038	0.228	-0.222
323.15	0.803	13.042	16.512	0.036	0.215	-0.086
323.15	0.605	9.759	16.475	0.037	0.224	-0.129
323.14	0.405	6.485	16.444	0.035	0.211	-0.133
323.15	0.200	3.188	16.420	0.034	0.207	-0.105
323.15	0.108	1.724	16.417	0.034	0.208	-0.052
473.14	1.798	19.652	23.342	0.042	0.181	-0.077
473.15	1.498	16.343	23.263	0.045	0.194	-0.229
473.15	1.200	13.065	23.216	0.043	0.183	-0.243
473.15	0.996	10.818	23.191	0.043	0.185	-0.222
473.15	0.797	8.646	23.159	0.041	0.179	-0.237
473.15	0.606	6.566	23.124	0.042	0.180	-0.273
473.15	0.400	4.335	23.101	0.043	0.186	-0.248
473.15	0.198	2.146	23.075	0.043	0.186	-0.242
473.15	0.100	1.080	23.069	0.043	0.188	-0.211
Reproducibility checks						
298.16	0.602	10.583	15.255	0.037	0.246	-0.277
298.16	0.405	7.071	15.212	0.039	0.256	-0.382
298.16	0.205	3.538	15.197	0.039	0.257	-0.312
298.16	0.105	1.815	15.188	0.037	0.242	-0.298

prediction values using the model [27]implemented in NIST REFPROP 10.0 [28,29] versus the temperature. The results were verified by comparing to very accurate data at zero-density calculated *ab initio* by Mehl et al. [51] and to data given by May et al. [52]. The deviation does not exceed 0.2% for neither the low- nor the high-pressure viscometer.

3.3. Dynamic viscosity data of $CO_2 + H_2$ mixtures

87 viscosity data points of the mixture CH07 and 78 viscosity data points of the mixtures CH20 are presented in Table 9 and Table 10, respectively. The data are reported in chronological order, starting at a temperature of 298 K followed by (323, 473 and 273) K and again 298 K for reproducibility check. The measurements were conducted in the gas and supercritical phases. The maximum pressure was different for each fluid composition, temperature, and viscometer due to the restrictions resulting from the phase boundary and the flow model. For instance, at 273 K, the mixture CH07 was measured up to 3.4 MPa for the high-pressure apparatus and 0.6 MPa for the low-pressure apparatus. In the former case the pressure was limited by the proximity to the phase

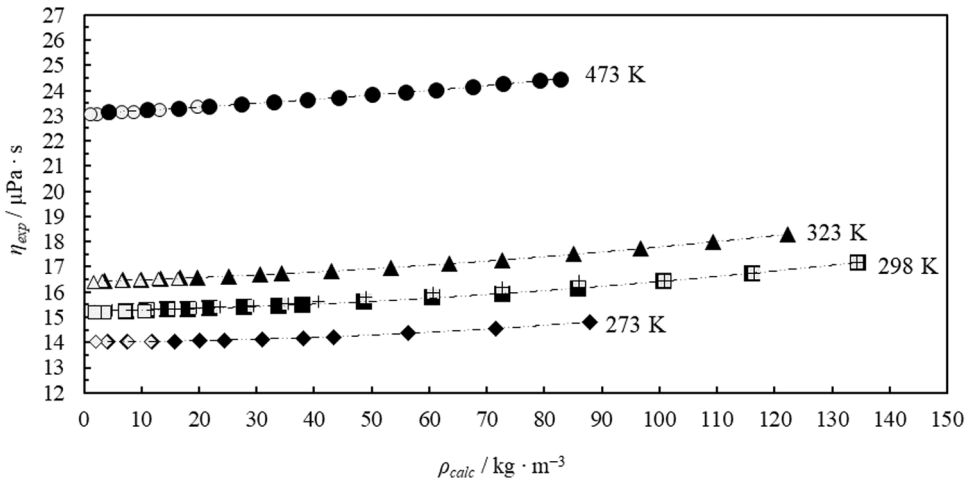

Fig. 12. Dynamic viscosity data for the mixture CN10 are plotted versus density of the mixture ρcalc, calculated with the GERG-2008 model [56] implemented in NIST REFPROP 10.0 [28,29]. 273 K - HPV (◆); 273 K - LPV (◇); 298 K – HPV (■); 298 K- LPV (□); 323 K – HPV (▲); 323 K – LPV (Δ); 473 K – HPV (●); 473 K – LPV (○); 298 K- reproducibility check (+). The dashed line corresponds to a second-order polynomial fit to the data.

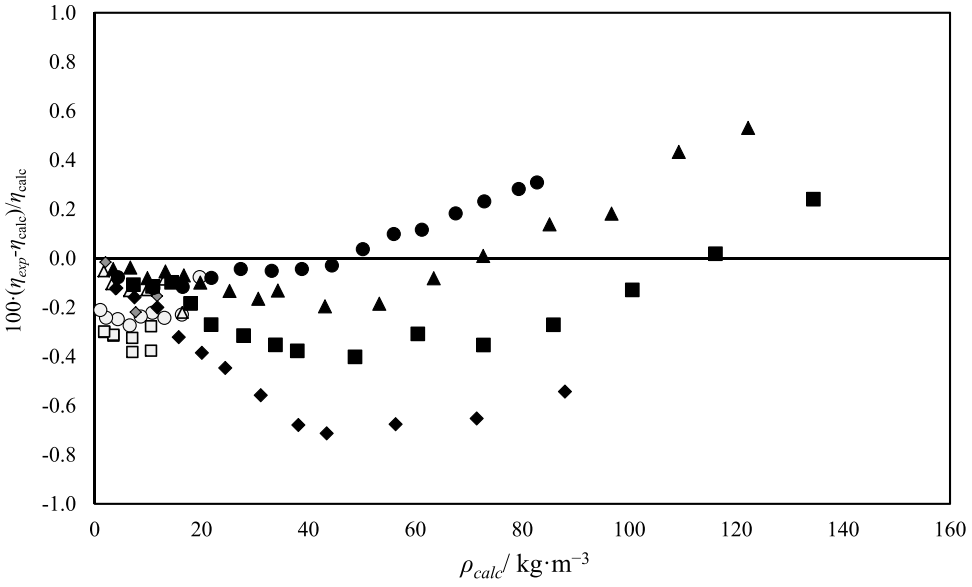

Fig. 13. Relative deviations between experimental and calculated viscosity values, ηexp and ηcalc, for the mixture CN10. ηcalc is calculated using the Extended Corresponding States (ECS) model [27] implemented in NIST REFPROP 10.0 [28,29]. Deviations are plotted versus density ρcalc density calculated from the GERG-2008 EOS [56] implemented in NIST REFPROP 10.0 [27,28]. 273 K - HPV (◆); 273 K - LPV (◇); 298 K – HPV (■); 298 K- LPV (□); 323 K – HPV (▲); 323 K – LPV (Δ); 473 K – HPV (●); 473 K – LPV (○).

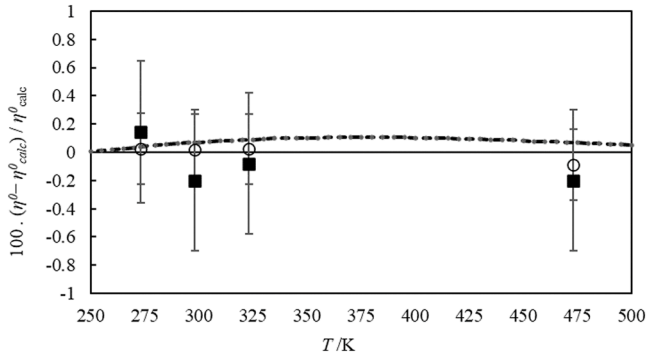

Fig. 14. Relative deviations between zero density viscosities η0 extrapolated from measurements and calculated values, ηcalc, for the mixture CN10. ηcalc is provided by the Extended Corresponding States (ECS) model [27] implemented in NIST REFPROP 10.0 [28,29]. Deviations are plotted versus the temperature T. Experimental viscosity measured in this work: HPV (■) and LPV (○). The dashed line corresponds to data by ab initio calculations [57] for this mixture. The error bars show the uncertainty estimated for each experimental data point.

boundary at 3.6 MPa and in the latter by the need to keep the Reynolds number below 30 [41]. The density ρ_{calc} was calculated from a new equations of state for H_2 binary mixtures [54], which was implemented in the thermodynamic software tool TREND 5.0 [55]. The dynamic viscosity data are plotted as a function of density as illustrated in Figs. 8 and 9. Just like for pure CO_2, an increase of temperature and density tends to increase the viscosity of CO_2-rich mixtures. Furthermore, it can be interpreted from the data that the viscosity changes considerable as the critical conditions are approached. Overall, in the low-density region, the impact of pressure on viscosity is not significant. The estimated maximum expanded relative combined uncertainty ($k = 2$) of the viscosity is 0.6% for data obtained from the high-pressure viscometer and 0.27% for data from the low-pressure viscometer. The results also show good agreement between the data obtained from the high-pressure viscometer and the low-pressure viscometer in the overlapping low-density region. The maximum difference between the data from the apparatuses occurs at 298 K with deviations of 0.19% and 0.29% for the mixtures CH07 and CH20, respectively. The differences are within the estimated uncertainties of the low-pressure apparatus. Regarding the reproducibility check at 298 K, a deviation of less than 0.05% was seen

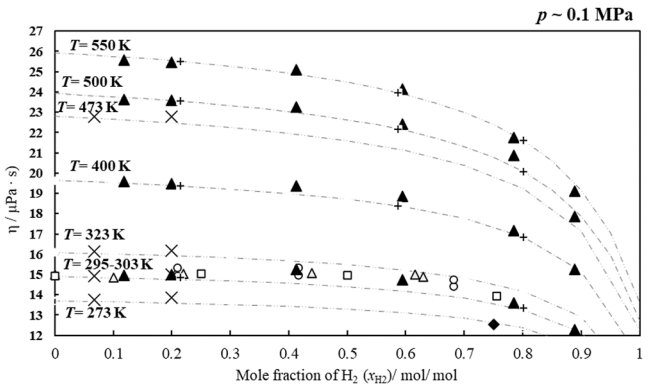

Fig. 15. Scenario 1: dynamic viscosity data versus the mole fraction of H2 in the binary mixture CO2 + H2 around 0.1 MPa and temperatures up to 550 K. This work (×);(▲); Trautz and Kurz (1931) [13] (×); Buddenberg and Wilke (1951) [14] (□); Golubev and Peteov (1959) [15] (◆); Gururaja et. al (1967) [16]; Saksena and Saxena (1968) [22] (○); Kestin et.al (1982) [58] (○). The dashed curves show the viscosity estimated by the extended corresponding states (ECS) model [27] implemented in NIST REFPROP 10.0 [28,29].

for the mixture CH07 using both apparatuses. With respect to the mixture CH20, 0.22% maximum deviation for the reproducibility check was observed when using the high-pressure viscometer and a 0.06% maximum deviation using the low-pressure viscometer was observed. The experimental viscosity data are also compared to the viscosity values estimated from the extended corresponding states (ECS) model [27] implemented in NIST REFPROP 10.0 [28,29]. The relative deviations from the model for four experimental isotherms are plotted against the density in Fig. 10 and Fig. 11. For both mixtures, the maximum deviation between the model and the data is less than 1.86%. It should be noted that the binary interaction parameters of the model were fitted only to a few old literature data on dilute gas viscosities [13]

.

3.4. Dynamic viscosity data of CO_2+ N_2 mixture

A total of 104 viscosity data points, 77 from the high-pressure viscometer and 27 from the low-pressure viscometer, were measured for the mixture CN10. Like for the H_2 mixtures, the measurements were performed at four isotherms and over a wide range of pressures up to 6 MPa. The results are reported in Table 11. The data of a reproducibility check at 298 K are included. The density of each data point was calculated from the GERG-2008 equation of state [56] implemented in the NIST REFPROP 10.0 [29]. The maximum relative expanded combined uncertainties (k = 2) of the reported viscosity values are 0.25% and 0.50% for data from the low pressure and high-pressure viscometers, respectively. For the reproducibility check at 298 K, a deviation between the original and reproduced viscosity values of 0.04% using the low-pressure viscometer and 0.50% using high pressure viscometer was observed, which is within the uncertainty of the measured data. The measured data are plotted in Fig. 12. Both apparatuses cover the low-density region up to 2 MPa and the corresponding data have a deviation of 0.25%, which is within the uncertainty of both apparatuses. The deviations between the measured viscosity data from this work and values from the model implemented in the NIST REFPROP 10.0 [28,29] are plotted in Fig. 13. These deviations vary between -0.713% and 0.531%. All four isotherms show a similar trend: negative relative deviation at low-densities up about 50 kg•m^{-3}, where the relative deviations as a function of density turn to a positive slope and increase for all isotherms. Noteworthy is the fact that there is an uncertainty of 5-10% in the model implemented in NIST REFPROP 10.0 [28,29] for all mixtures, since the specific interaction parameters for each mixture are not included in the model. The measured dynamic viscosity data has been extrapolated to zero density. The deviations between the extrapolated zero-density viscosity within this work and accurate data $\eta^0_{\text{ab initio}}$ generated by *ab initio* calculations for the mixture CO_2 + N_2 are plotted

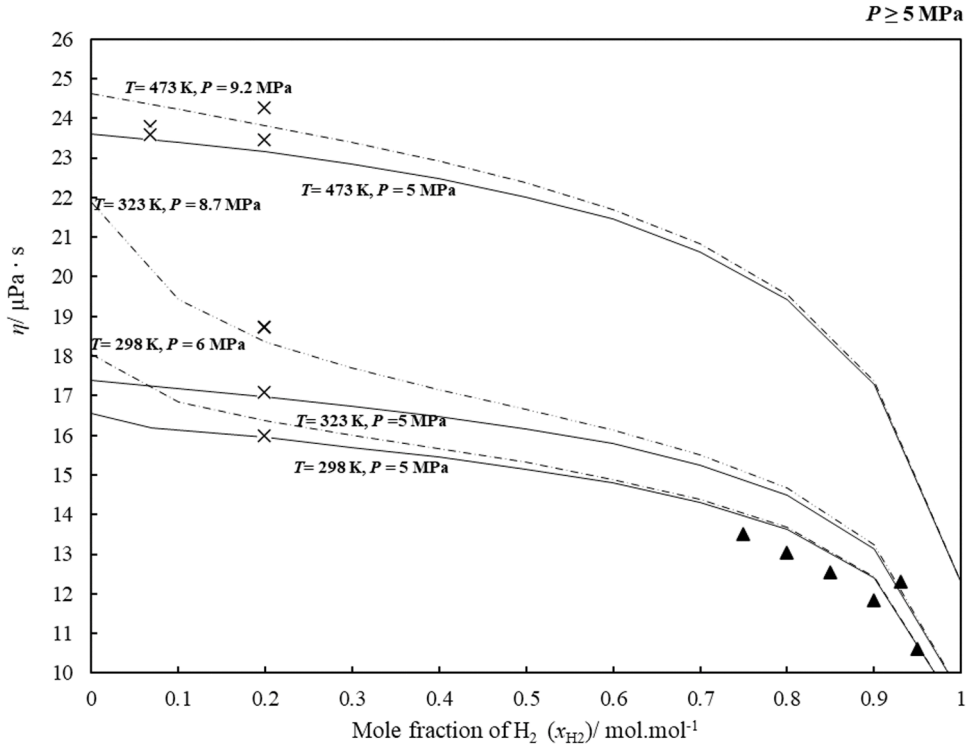

Fig. 16. Scenario 2: dynamic viscosity data versus the mole fraction of H2 in the binary mixture CO2 + H2 at p ≥ 5 MPa and temperatures up to 473 K. This work (×); Golubev and Peteov (1959) [15] (▲). The solid and dash curves are viscosity values estimated by the extended corresponding states (ECS) model [27] implemented in NIST REFPROP 10.0 [28,29] at 5 MPa maximum measured pressure within this work, respectively, as indicated by the labels.

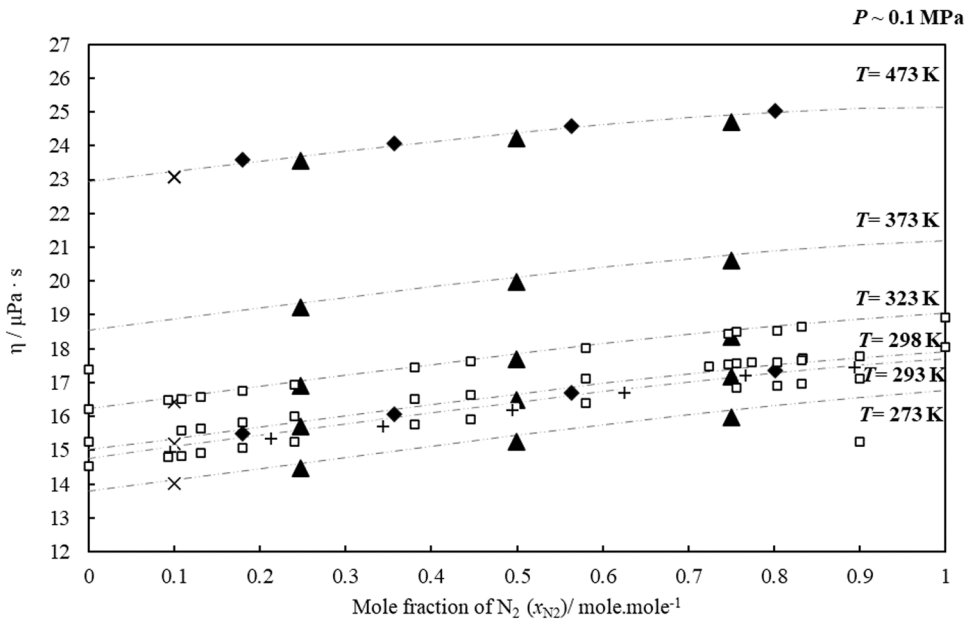

Fig. 17. Scenario 1: dynamic viscosity data versus the mole fraction of N2 for CO2 + N2 mixtures at p = 0.1 MPa and in the temperature range 273 K to 473 K. This work (×); Kestin et. al (1959) at 293 K [24]; Kestin et. al (1974 and 1966) [20,25] (◆) and [21]; Munczak and Hochrainer (1969) [26] (□); Humberg (2020) [21] (▲). The dashed curves correspond to the extended corresponding states (ECS) model estimates [27] implemented in NIST REFPROP 10.0 [28,29].

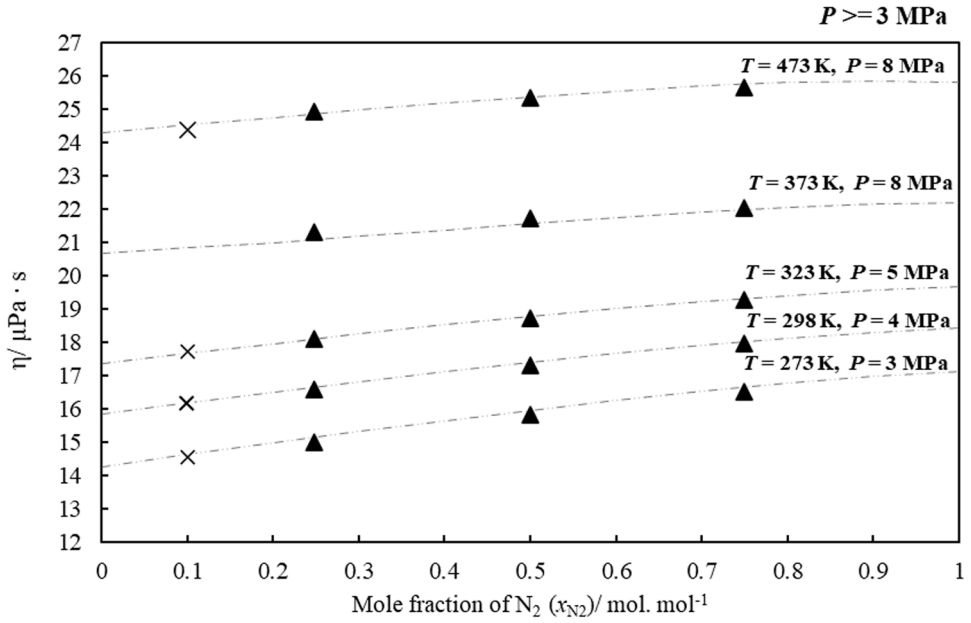

Fig. 18. Scenario 2: dynamic viscosity data versus the composition of N2 in the binary mixture CO2 + N2 at 3 ≤ p ≤ 8 MPa for isotherms (273, 298, 323 and 473) K. This work (×); Humberg (2020) [21] (▲). The dashed curves correspond to the extended corresponding states (ECS) model estimates [27] implemented in NIST REFPROP 10.0 [28,29].

in Fig. 14. The deviations are within the uncertainty of experimental measurements. There is also a good fit between the two models.

3.5. Impact of H_2 and N_2 impurities on the viscosity of CO_2-rich mixtures

Several studies [9,10], have shown that the impact of impurities on CO_2 streams needs to be understood as CCS processes cover a broad range of fluid conditions and involve multi-component mixtures. For this purpose, experimental viscosity data for CO_2 + H_2 and CO_2 + N_2 mixtures at different pressures, temperatures and mixture compositions from different sources were compiled together with the data presented in this work. In addition, data calculated from the Extended Corresponding States (ECS) model [27] implemented in NIST REFPROP 10.0 [28,29] were used to see the behaviour of viscosity change with composition at different temperatures and pressures, in particular, where experimental data are missing. In the following, two scenarios with different pressure regions were investigated. The first scenario evaluated the viscosity change with composition at a pressure around 0.1 MPa. The reason for choosing such a low-pressure threshold is that there are several data points at this pressure in the literature. The second scenario considers higher pressures. The highest pressure is in the range of the maximum pressure measured in this work since it is difficult to

find sufficient data in the literature at higher pressures to cover the whole composition range. The two scenarios were applied for both systems, $CO_2 + H_2$ and $CO_2 + N_2$.

$CO_2 + H_2$: The gas viscosity of pure H_2 is smaller than the one of pure CO_2 at the same pressure and temperature mainly due to lower molecular weight. The viscosity of CO_2 + H_2 mixtures is reduced with increasing H_2 content, as shown in Fig. 15 and Fig. 16. However, most of the reduction in viscosity occurs at high hydrogen mole fractions. As shown in Fig. 15 for around 0.1 MPa, the reduction in viscosity from pure CO_2 to a mixture with a hydrogen mole fraction of 0.5 does not exceed 6% over the whole temperature range studied. A similar trend is observed between 6 and 9.2 MPa at 473 K as seen in Fig. 16. But at a pressure of 8.7 MPa and a temperature of 323 K the reduction of viscosity from pure CO_2 is already 17% at a hydrogen mole fraction of 0.2, according to ECS. This could be due to critical enhancement effect, although there is no data backing up the model directly in this region close to the critical point of CO_2. It can be concluded that the impact of H_2 on the viscosity of CO_2-rich mixtures is not major in the gas phase and low-density supercritical phase, except close to the critical point. To complement these results, Ref. [19], which used a capillary tube viscosity measurement method, shows a significant reduction in viscosity when adding small amounts of hydrogen also at pressures 2 to 3 MPa above the critical pressure in a temperature region around the critical point. For instance, at a pressure around 11 MPa, viscosities at a hydrogen mole fraction of 0.05 were about 10% and 30% lower than for pure CO_2 at 288.15 K and 323.15 K, respectively.

$CO_2 + N_2$: Opposite to H_2, adding N_2 to CO_2 in the gas phase increases the viscosity for the investigated conditions as seen from Fig. 17 and Fig. 18. The interpretation is that the viscosities of CO_2 + N_2 mixtures behave ideal with the mole fraction of N_2 at both low- and high-pressure ranges. N_2 mole fractions of 0. 1 and 0.25 lead to a viscosity that is 3% and 6.5% higher compared to pure CO_2, respectively.

In addition, these figures show the consistency between the measured data within this research work and both available experimental data and the data estimated by the model. The only exception is the data produced by [26] in 1969, where the viscosity data at 323 K are not consistent with the data from other literature, models as well as data produced from this work. Moreover, this analysis highlights the need of the viscosity measurement at supercritical phase and close to the critical point.

4. Conclusion

In this work, viscosity measurements were investigated for three binary CO_2-rich mixtures with mole fractions of 0.07 H_2, 0.20 H_2 and 0.10 N_2, respectively. The measurements were performed at in total 269 data points from 0.1 MPa using a low-pressure viscometer to higher pressures, up to 9.25 MPa for the mixture CH20, using a high pressure-viscometer. The temperature range for the viscosity measurements was 273 to 473 K. The experimental data within this work are consistent with data from existing literature sources and with values calculated using the extended corresponding states (ECS) model implemented in the NIST REFPROP 10.0 [28,29]. Extrapolated zero- density viscosity data for the mixture CN10 also show a very good agreement with accurate data calculated by *ab initio* approaches with a maximum deviation of 0.2 %. Finally, it was seen that the viscosity of CO_2-rich mixtures is more strongly affected by the presence of N_2 as impurity, than by hydrogen.

However, experimental viscosity data in dense phase, liquid and, in particular, close to critical region as well as data for multi-component mixtures are still missing to a great extent. Consequently, the viscosity models are suffering from the lack of experimental data. Hence, further experimental and modelling studies at high pressures and improved viscosity models can pave the path to improve CO_2 reservoir modelling (Eqn. 1–8).

Declaration of Competing Interest

The authors declare that they have no known competing financial interests or personal relationships that could have appeared to influence the work reported in this paper.

Acknowledgment

This PhD project of Bahareh Khosravi is support from the research program CLIMIT and the NCCS Centre, performed under the Norwegian research program Centres for Environment-friendly Energy Research (FME). The authors acknowledge the following partners for their contributions: Aker Carbon Capture, Allton, Ansaldo Energia, Baker Hughes, CoorsTek Membrane Sciences, Equinor, Fortum Oslo Varme, Gassco, KROHNE, Larvik Shipping, Lundin Norway, Norcem, Norwegian Oil and Gas, Quad Geometrics, Stratum Reservoir, Total, Vår Energi, Wintershall DEA, and the Research Council of Norway (257579/E20 and 280394). The contribution of Benjamin Betken was in part supported by the Fraunhofer High-Performance Center DYNAFLEX and the German State of North Rhine-Westphalia.

References

[1] S. Peletiri, N. Rahmanian, I. Mujtaba, CO2 pipeline design: a review, Energies 11 (9) (2018) 2184, https://doi.org/10.3390/en11092184.
[2] Y. Tan, W. Nookuea, H. Li, E. Thorin, J. Yan, Property impacts on carbon capture and storage (CCS) processes: a review, Energy Convers. Manage. 118 (2016) 204–222, https://doi.org/10.1016/j.enconman.2016.03.079.
[3] M.J. Patel, E.F. May, M.L. Johns, High-fidelity reservoir simulations of enhanced gas recovery with supercritical CO2, Energy 111 (2016) 548–559. http://doi.org/10.1016/j.energy.2016.04.120.
[4] G. Skaugen, S. Roussanaly, J. Jakobsen, A. Brunsvold, Techno-economic evaluation of the effects of impurities on conditioning and transport of CO2 by pipeline, Int. J. Greenhouse Gas Control 54 (2016) 627–639, https://doi.org/10.1016/j.ijggc.2016.07.025.
[5] S.T. Munkejord, M. Hammer, S.W. Løvseth, CO2 transport: data and models–a review, Appl. Energy 169 (2016) 499–523, https://doi.org/10.1016/j.apenergy.2016.01.100.
[6] H. Li, Ø. Wilhelmsen, Y. Lv, W. Wang, J. Yan, Viscosities, thermal conductivities and diffusion coefficients of CO2 mixtures: review of experimental data and theoretical models, Int. J. Greenhouse Gas Control 5 (5) (2011) 1119–1139, https://doi.org/10.1016/j.ijggc.2011.07.009.
[7] J. M. Nordbotten, M. A. Celia, and S. Bachu, "Injection and storage of CO 2 in deep saline aquifers: analytical solution for CO2 plume evolution during injection," *Transport in Porous media*, vol. 58, no. 3, pp. 339–360, 2005, doi: https://doi.org/10.1007/s11242-004-0670-9.
[8] C. Eickhoff, et al., IMPACTS: economic trade-offs for CO2 impurity specification, Energy Procedia 63 (2014) 7379–7388, https://doi.org/10.1016/j.egypro.2014.11.774.
[9] H. Li, Ø. Wilhelmsen, J. Yan, Properties of CO2 mixtures and impacts on carbon capture and storage, Handbook of Clean Energy Systems (2015) 1–17, https://doi.org/10.1002/9781118991978.hces038.
[10] B. Wetenhall, et al., Impact of CO2 impurity on CO2 compression, liquefaction and transportation, Energy Procedia 63 (2014) 2764–2778, https://doi.org/10.1016/j.egypro.2014.11.299.
[11] S.W. Løvseth, ImpreCCS: Lower CCS cost and risk through better CO2 viscosity and thermal conductivity knowledge, SINTEFblog (2019). https://blog.sintef.com/sintefenergy/impreccs-lower-ccs-cost-risk-co2-viscosity-thermal-conductivity/(accessed.
[12] K. Espegren, S. Damman, P. Pisciella, I. Graabak, A. Tomasgard, The role of hydrogen in the transition from a petroleum economy to a low-carbon society, Int. J. Hydrogen Energy 46 (45) (2021) 23125–23138, https://doi.org/10.1016/j.ijhydene.2021.04.143.
[13] M. Trautz, F. Kurz, Die Reibung, Wärmeleitung und Diffusion in Gasmischungen XV. Die Reibung von H2, N2O, CO2 und C3H8 und ihren binären Gemischen, Ann. Phys. 401 (8) (1931) 981–1003, https://doi.org/10.1002/andp.19314010808.
[14] C. Wilke, A viscosity equation for gas mixtures, J. Chem. Phys. 18 (4) (1950) 517–519, https://doi.org/10.1063/1.1747673.
[15] I.F. Golubev, Viscosity of gases and gas mixtures: A handbook, Israel program for scientific translations, Jerusalem, 1970.
[16] G. Gururaja, M. Tirunarayanan, A. Ramachandran, Dynamic viscosity of gas mixtures, J. Chem. Eng. Data 12 (4) (1967) 562–567.
[17] J. Kestin, S. Ro, W. Wakeham, The transport properties of binary mixtures of hydrogen with CO, CO2 and CH4, Physica A 119 (3) (1983) 615–638, https://doi.org/10.1016/0378-4371(83)90113-9.
[18] V.A. Mal'tsev, et al., Viscosity of H2− CO2 Mixtures at (500, 800, and 1100) K, J. Chem. Eng. Data 49 (3) (2004) 684–687, https://doi.org/10.1021/je0342419.
[19] I. Al-Siyabi, Doctoral Thesis, Heriot-Watt University, 2013.

[20] J. Kestin, S.T. Ro, The viscosity of nine binary and two ternary mixtures of gases at low density, Ber. Bunsenges. Phys. Chem. 78 (1) (1974) 20–24, https://doi.org/10.1002/bbpc.19740780104.
[21] K. Humberg, Doctoral Thesis, Fakultät für Maschinenbau, Bochum, Ruhr-Universität Bochum, 2020, pp. 294–77103.
[22] S.C. M. P. S. Saksena, Viscosity of multicomponent gas mixtures, Proceedings Nat. Inst. Sci. India. Part A, Phys. sci. 31 (1) (1965) 18–25.
[23] S. Cheng, et al., Viscosity Measurements of the H2–CO2, H2–CO2–CH4, and H2–H2O Mixtures and the H2–CO2–CH4–CO–H2O System at 280–924 K and 0.7–33.1 MPa with a Capillary Apparatus, J. Chem. Eng. Data 65 (8) (2020) 3834–3847, https://doi.org/10.1021/acs.jced.0c00176.
[24] J. Kestin, W. Leidenfrost, The effect of pressure on the viscosity of N2CO2 mixtures, Physica 25 (1-6) (1959) 525–536, https://doi.org/10.1016/S0031-8914(59)95498-9.
[25] J. Kestin, Y. Kobayashi, R. Wood, The viscosity of four binary, gaseous mixtures at 20 and 30 C, Physica 32 (6) (1966) 1065–1089, https://doi.org/10.1016/0031-8914(66)90143-1.
[26] D. F. H. Munczak, Viscosity measurements of dry and wet nitrogen-carbon dioxide mixtures, Sitzungsber. Oesterr. Akad. Wiss., Math.-Naturwiss II (177) (1968) 21–30. Abt.
[27] J.F. Ely, H. Hanley, Prediction of transport properties. 1. Viscosity of fluids and mixtures, Industrial Eng. Chem. Fundamentals 20 (4) (1981) 323–332, https://doi.org/10.1021/i100004a004.
[28] M. L. Huber, "Models for viscosity, thermal conductivity, and surface tension of selected pure fluids as implemented in REFPROP v10. 0," 2018, doi: https://doi.org/10.6028/NIST.IR.8209.
[29] E.W. Lemmon, M.L. Huber, M.O. McLinden, NIST standard reference database 23: reference fluid thermodynamic and transport properties-REFPROP, Version 10.0, Nat. Inst. Standards Technol. (8.0) (2018), https://doi.org/10.18434/T4/1502528.
[30] A. Docter, H. Lösch, W. Wagner, A new apparatus for combined measurements of the viscosity and density of fluids for temperatures from 233 to 523 K at pressures up to 30 MPa, Int. J. Thermophys. 20 (2) (1999) 485–505, https://doi.org/10.1023/A:1022601003582.
[31] C. Evers, H. Lösch, W. Wagner, An absolute viscometer-densimeter and measurements of the viscosity of nitrogen, methane, helium, neon, argon, and krypton over a wide range of density and temperature, Int. J. Thermophys. 23 (6) (2002) 1411–1439, https://doi.org/10.1023/A:1020784330515.
[32] M. Schäfer, Doctoral Thesis, Ruhr-Universität Bochum, 2016.
[33] R. Span, J. Gernert, A. Jäger, Accurate thermodynamic-property models for CO2-rich mixtures, Energy Procedia 37 (2013) 2914–2922, https://doi.org/10.1016/j.egypro.2013.06.177.
[34] R.F. Berg, M.R. Moldover, Recommended viscosities of 11 dilute gases at 25 C, J. Phys. Chem. Ref. Data 41 (4) (2012), 043104, https://doi.org/10.1063/1.4765368.
[35] W. Cencek, M. Przybytek, J. Komasa, J.B. Mehl, B. Jeziorski, K. Szalewicz, Effects of adiabatic, relativistic, and quantum electrodynamics interactions on the pair potential and thermophysical properties of helium, J. Chem. Phys. 136 (22) (2012), 224303, https://doi.org/10.1063/1.4712218.
[36] B. Mangum, The new International Temperature Scale of 1990 (ITS-90), Clin. Chem. 35 (3) (1989) 503–505, https://doi.org/10.1093/clinchem/35.3.503.
[37] DIN EN ISO 6143, Gas analysis – Comparison Methods for Determining and Checking the Composition of Calibration Gas Mixtures (ISO 6143:2001), 2006, European Committee for Standardization, Brussels, 2006 [Online]. Available, https://standards.iteh.ai/catalog/standards/cen/2d3fc86a-76a7-47d1-9388-672d9e957061/en-iso-6143-2006.
[38] R.J. Donnelly, K. Schwarz, Experiments on the stability of viscous flow between rotating cylinders-VI. Finite-amplitude experiments, Proceedings of the Royal Society of London. Series A. Mathematical and Physical Sciences 283 (1395) (1965) 531–556, https://doi.org/10.1098/rspa.1965.0044.
[39] "ISO International Organization for Standardization, Uncertainty of measurement – Part3: Guide to the expression of uncertainty in measurement.," 2008. [Online]. Available: https://www.iso.org/standard/50461.html.
[40] M. Schäfer, M. Richter, R. Span, Measurements of the viscosity of carbon dioxide at temperatures from (253.15 to 473.15) K with pressures up to 1.2 MPa, The Journal of Chemical Thermodynamics 89 (2015) 7–15, https://doi.org/10.1016/j.jct.2015.04.015.
[41] K. Humberg, M. Richter, J.M. Trusler, R. Span, Measurement and modeling of the viscosity of (nitrogen+ carbon dioxide) mixtures at temperatures from (253.15 to 473.15) K with pressures up to 2 MPa, The Journal of Chemical Thermodynamics 120 (2018) 191–204, https://doi.org/10.1016/j.jct.2018.01.015.
[42] J.W. Leachman, R.T. Jacobsen, S. Penoncello, E.W. Lemmon, Fundamental equations of state for parahydrogen, normal hydrogen, and orthohydrogen, J. Phys. Chem. Ref. Data 38 (3) (2009) 721–748, https://doi.org/10.1063/1.3160306.
[43] A.K. Barua, M. Afzal, G.P. Flynn, J. Ross, Viscosity of Hydrogen, Deuterium, Methane, and Carbon Monoxide from—50° to 150°C below 200 Atmospheres, J. Chem. Phys. 41 (2) (1964) 374–378, https://doi.org/10.1063/1.1725877.
[44] C.D. Muzny, M.L. Huber, A.F. Kazakov, Correlation for the viscosity of normal hydrogen obtained from symbolic regression, J. Chem. Eng. Data 58 (4) (2013) 969–979, https://doi.org/10.1021/je301273j.
[45] S.-Y. Chuang, P.S. Chappelear, R. Kobayashi, Viscosity of methane, hydrogen, and four mixtures of methane and hydrogen from-100. degree. C to 0. degree. C at high pressures, J. Chem. Eng. Data 21 (4) (1976) 403–411, https://doi.org/10.1021/je60071a010.
[46] J. Gracki, G. Flynn, J. Ross, Viscosity of Nitrogen, Helium, Hydrogen, and Argon from− 100 to 25 c up to 150–250 atm, J. Chem. Phys. 51 (9) (1969) 3856–3863, https://doi.org/10.1063/1.1672602.
[47] M. Hongo, H. Iwasaki, Viscosity of hydrogen and of hydrogen-ammonia mixtures under pressures, The Review of Physical Chemistry of Japan 48 (1) (1978) 1–9 [Online]. Available, http://hdl.handle.net/2433/47056.
[48] A. Michels, A. Schipper, W. Rintoul, The viscosity of hydrogen and deuterium at pressures up to 2000 atmospheres, Physica 19 (1-12) (1953) 1011–1028, https://doi.org/10.1016/S0031-8914(53)80112-6.
[49] H. Nabizadeh, F. Mayinger, Viscosity of Gaseous R404A, R407C, R410A, and R507, Int. J. Thermophys. 20 (3) (1999) 777–790, https://doi.org/10.1023/A:1022618832289.
[50] N. Sakoda, T. Hisatsugu, K. Furusato, K. Shinzato, M. Kohno, Y. Takata, Viscosity measurements of hydrogen at high temperatures up to 573 K by a curved vibrating wire method, The Journal of Chemical Thermodynamics 89 (2015) 22–26, https://doi.org/10.1016/j.jct.2015.04.028.
[51] J.B. Mehl, M.L. Huber, A.H. Harvey, Ab initio transport coefficients of gaseous hydrogen, Int. J. Thermophys. 31 (4) (2010) 740–755, https://doi.org/10.1007/s10765-009-0697-9.
[52] E.F. May, R.F. Berg, M.R. Moldover, Reference viscosities of H2, CH4, Ar, and Xe at low densities, Int. J. Thermophys. 28 (4) (2007) 1085–1110, https://doi.org/10.1007/s10765-007-0198-7.
[53] M. Assael, S. Mixafendi, W.A. Wakeham, The viscosity and thermal conductivity of normal hydrogen in the limit of zero density, J. Phys. Chem. Ref. Data 15 (4) (1986) 1315–1322, https://doi.org/10.1063/1.555764.
[54] R. Beckmüller, M. Thol, I. Bell, E. Lemmon, R. Span, New Equations of State for Binary Hydrogen Mixtures Containing Methane, Nitrogen, Carbon Monoxide, and Carbon Dioxide, J. Phys. Chem. Ref. Data 50 (1) (2021), 013102, https://doi.org/10.1063/5.0040533.
[55] TREND 5.0, Thermodynamic Reference and Engineering Data 4.0, Lehrstuhl für Thermodynamik, Ruhr-Universität Bochum, 2019.
[56] O. Kunz, R. Klimeck, W. Wagner, M. Jaeschke, *The GERG-2004 wide-range equation of state for natural gases and other mixtures*. Germany, 2007.
[57] J.-P. Crusius, R. Hellmann, J.C. Castro-Palacio, V. Vesovic, Ab initio intermolecular potential energy surface for the CO2—N2 system and related thermophysical properties, J. Chem. Phys. 148 (21) (2018), 214306, https://doi.org/10.1063/1.5034347.
[58] J. Kestin, S. Ro, W. Wakeham, The Viscosity of Carbon-Monoxide and its Mixtures with Other Gases in the Temperature Range 25–200°C, Ber. Bunsenges. Phys. Chem. 86 (8) (1982) 753–760.